

DOCUMENT CONTROL DATA - R&D

(Security classification of title, body of abstract and indexing annotation must be entered when the overall report is classified).

1. ORIGINATING ACTIVITY (Corporate author) Air Force Cambridge Research Laboratories (LYB) L.G. Hanscom Field Bedford, Massachusetts 01730	2a. REPORT SECURITY CLASSIFICATION Unclassified
	2b. GROUP

3. REPORT TITLE  
SPECTRAL CHARACTERISTICS OF SURFACE-LAYER TURBULENCE

4. DESCRIPTIVE NOTES (Type of report and inclusive dates)  
Scientific. Interim.

5. AUTHOR(S) (First name, middle initial, last name)  
J. C. Kaimal                      Y. Izumi  
J. C. Wyngaard                O. R. Coté

6. REPORT DATE 29 August 1972	7a. TOTAL NO. OF PAGES 27	7b. NO. OF REFS 37
----------------------------------	------------------------------	-----------------------

8a. CONTRACT OR GRANT NO.  b. PROJECT, TASK, WORK UNIT NO. 7655-02-01  c. DOD ELEMENT 62101F  d. DOD SUBELEMENT 681300	9a. ORIGINATOR'S REPORT NUMBER(S) AFCRL-72-0492
	9b. OTHER REPORT NO(S) (Any other numbers that may be assigned this report)

10. DISTRIBUTION STATEMENT  
Approved for public release; distribution unlimited.

11. SUPPLEMENTARY NOTES Reprinted from the Quarterly Journal of the Royal Meteorological Society, Vol. 98, No. 417, July 1972.	12. SPONSORING MILITARY ACTIVITY Air Force Cambridge Research Laboratories (LYB) L.G. Hanscom Field Bedford, Massachusetts 01730
---	---

13. ABSTRACT

The behaviour of spectra and cospectra of turbulence in the surface layer is described within the framework of similarity theory using wind and temperature fluctuation data obtained in the 1968 AFCRL Kansas experiments. With appropriate normalization, the spectra and cospectra are each reduced to a family of curves which spread out according to  $z/L$  at low frequencies but converge to a single universal curve in the inertial subrange. The paper compares these results with data obtained by other investigators over both land and water.

Spectral constants for velocity and temperature are determined and the variability in the recent estimates of the constants is discussed. The high-frequency behaviour is consistent with local isotropy. In the inertial subrange, where the spectra fall as  $n^{-5/3}$ , the cospectra fall faster;  $uw$  and  $w\theta$  as  $n^{-7/3}$ , and  $u\theta$ , on the average, as  $n^{-5/2}$ . The  $4/3$  ratio between the transverse and longitudinal spectral levels is observed at wavelengths of the order of the height above ground under unstable conditions and at wavelengths of the order of  $L/10$  under stable conditions. This lower isotropic limit is shown to be governed by the combined effects of shear and buoyancy on small-scale eddies.

Reproduced by  
NATIONAL TECHNICAL  
INFORMATION SERVICE  
U.S. Department of Commerce  
Springfield, VA 22151

KEY WORDS: Atmospheric turbulence, Surface layer, Spectra, Cospectra

AD 748543

## Spectral characteristics of surface-layer turbulence

J. C. KAIMAL, J. C. WYNGAARD, Y. IZUMI and O. R. COTÉ  
Air Force Cambridge Research Laboratories, Bedford, Massachusetts

(Manuscript received 5 October 1971; in revised form 28 February 1972. Communicated by Dr. R. Shapiro)

## SUMMARY

The behaviour of spectra and cospectra of turbulence in the surface layer is described within the framework of similarity theory using wind and temperature fluctuation data obtained in the 1968 AFCRL Kansas experiments. With appropriate normalization, the spectra and cospectra are each reduced to a family of curves which spread out according to  $z/L$  at low frequencies but converge to a single universal curve in the inertial subrange. The paper compares these results with data obtained by other investigators over both land and water.

Spectral constants for velocity and temperature are determined and the variability in the recent estimates of the constants is discussed. The high-frequency behaviour is consistent with local isotropy. In the inertial subrange, where the spectra fall as  $n^{-5/3}$ , the cospectra fall faster:  $uw$  and  $w\theta$  as  $n^{-7/3}$ , and  $u\theta$ , on the average, as  $n^{-3/2}$ . The  $4/3$  ratio between the transverse and longitudinal spectral levels is observed at wavelengths of the order of the height above ground under unstable conditions and at wavelengths of the order of  $L/10$  under stable conditions. This lower isotropic limit is shown to be governed by the combined effects of shear and buoyancy on small-scale eddies.

## 1. INTRODUCTION

Since the early 1950's, when modern recording and computing techniques became available, considerable effort has gone into the study of atmospheric turbulence and its spectral characteristics. The large amounts of data collected to date by various investigators show clear indication that spectra of wind velocity and temperature obey similarity theory over a range of frequencies in the surface layer. The 1968 AFCRL (Air Force Cambridge Research Laboratories) experiment in Kansas (Haugen, Kaimal and Bradley 1971) was an attempt to obtain a comprehensive set of data on wind and temperature fluctuations over a flat, uniform site. In this paper we will use the framework of similarity theory to describe the spectra and cospectra in the surface layer over a broad range of stability conditions and to compare them with results obtained by other investigators.

Instrumentation for the Kansas experiment included three-axis sonic anemometers, hot-wire anemometers and fine platinum wire thermometers mounted at three levels (5.66, 11.3 and 22.6 m) on a 32 m tower. Surface stress measurements were obtained from two CSIRO drag plates (Bradley 1968) installed about 50 and 80 m to one side of the tower. Mean wind speed and temperature gradients were measured with standard cup anemometers and resistance thermometers at 8 levels on the tower between 2.0 and 32 m.

Outputs from these sensors were sampled, digitized and stored on magnetic tape by means of a computer-controlled data acquisition system (Kaimal, Haugen and Newman 1966). Analog signals from the sonic and hot-wire anemometers, the fine platinum wire thermometers and the drag plates were sampled 20 times a second. The hot-wire anemometer signals were also differentiated, low-pass filtered (Wyngaard and Lumley 1967) and recorded on an FM tape recorder. Further details of the site, instrumentation and data handling can be found in the earlier paper by Haugen *et al.* (1971).

## 2. DATA ANALYSIS

Fifteen 1-hr runs, 10 unstable and 5 stable, were selected for analysis. With data from three levels they comprise a large set of spectra and cospectra covering a range of  $z/L$  values from  $-2.1$  to  $+3.3$ . The distribution of the runs according to categories of  $z/L$  is given in Table 1. Mean profiles, variances, correlations and other statistical parameters for each of these runs are presented in a separate data report (Izumi 1971).

TABLE 1. RUN NUMBERS SEPARATED ACCORDING TO  $z/L$  CATEGORIES. THE FIRST NUMBER DENOTES THE RUN; THE NUMBERS 1, 2 AND 3 WITHIN PARENTHESES DENOTE LEVELS 5.66, 11.3 AND 22.6 m RESPECTIVELY

$z/L$ Range	Runs (1 hr each)
< -2.0	19(3), 28(3)
-2.0 to -1.0	19(2), 20(3), 28(2)
-1.0 to -0.5	13(3), 14(3), 19(1), 20(2), 28(1), 30(3), 40(3)
-0.5 to -0.3	13(2), 14(2), 20(1), 21(3), 30(2), 40(2), 48(3)
-0.3 to -0.1	13(1), 14(1), 21(1), 21(2), 30(1), 31(2), 31(3), 40(1), 48(1), 48(2)
-0.1 to 0	31(1)
0 to +0.1	37(1)
+0.1 to +0.3	17(1), 24(1), 25(1), 25(2), 37(2)
+0.3 to +0.5	17(2), 17(3), 24(2), 25(3), 37(3)
+0.5 to +1.0	23(1), 24(3)
+1.0 to +2.0	23(2)
> +2.0	23(3)

The spectra and cospectra were computed using the fast-Fourier technique. The available bandwidth was covered in two stages. The higher range (0.005 to 10 Hz) was obtained by dividing each 1-hr record into 16 consecutive blocks of 4,096 data points and constructing a composite spectrum by averaging the 16 separate spectra. The composite spectrum was then smoothed by averaging spectral estimates over frequency bands.

For the lower range (0.0003 to 0.6 Hz) a new time series was generated from the original series by subjecting it to a 16-point non-overlapping block average. The spectrum computed from this series has inherently more scatter than the composite spectrum but the agreement between the two in the two decades where they overlap is very good. The higher range was, therefore, treated as our basic spectrum with estimates from the lower range used only to extend its bandwidth to 0.0003 Hz.

Friction velocity ( $u_*$ ) values were derived from the average of two drag plate readings as described by Haugen *et al.* (1971). Dissipation rate ( $\epsilon$ ) values were obtained from the variance of the differentiated hot-wire anemometer signals (Wyngaard and Coté 1972). Wind and temperature gradients were computed from the profile data by differentiating curves fitted at 5 points, 2 above and 2 below the reference level (Businger, Wyngaard, Izumi and Bradley 1971).

The symbols used are standard except where noted.  $U$  is the mean horizontal wind vector;  $u$ ,  $v$ , and  $w$  are the fluctuating velocity components along the longitudinal ( $x$ ), lateral ( $y$ ) and vertical ( $z$ ) directions.  $\Theta$  denotes the mean potential temperature and  $\theta$  its fluctuating component at any level.  $\bar{\Theta}$  represents the average potential temperature for the entire layer. Scaling temperature  $T_*$  is defined as  $-\overline{w\theta}/u_*$ ,  $N$  is the dissipation rate for  $\bar{\theta}^2/2$  and  $k$  is the von Kármán's constant. For reasons of symmetry, this definition for  $T_*$  is preferred over the one with  $k$  in the denominator. The dimensionless terms used here are

$f$	$=$	$nz/U$	a dimensionless frequency
$z/L$	$=$	$kz(g/\bar{\Theta})(T_*/u_*^2)$	a dimensionless height
$\phi_\epsilon$	$=$	$kz\epsilon/u_*^3$	a dimensionless dissipation rate for turbulent energy
$\phi_N$	$=$	$kzN/u_*T_*^2$	a dimensionless dissipation rate for temperature variance
$\phi_m$	$=$	$kz(dU/dz)/u_*$	a dimensionless velocity gradient
$\phi_h$	$=$	$kz(d\Theta/dz)/T_*$	a dimensionless temperature gradient

In the discussions to follow we will use symbols and plots most commonly used in atmospheric work. We measure frequency, not wavenumber, spectra and the conversion from one to the other is made through the use of Taylor's hypothesis. Strictly speaking we should use different symbols to represent the two types of spectra. Taking the  $u$  spectrum as an example

$$\int_0^{\infty} F_u(\kappa_1) \kappa_1^{-2} d\kappa_1 = \overline{u^2} = \int_0^{\infty} S_u(n) dn.$$

If  $\kappa_1 = 2\pi n/U$  we have

$$\frac{2\pi}{U} F_u\left(\frac{2\pi n}{U}\right) = S_u(n),$$

$$F_u(\kappa_1) = n S_u(n). \quad (1)$$

It is traditional in atmospheric work to plot frequency spectra, e.g.  $S_u(n)$  and  $n S_u(n)$ , not against  $n$  but against the nondimensional frequency,  $f$ . This convention will be followed in our paper. The spectral forms involving the product with  $n$  will be referred to as 'logarithmic' spectra and cospectra.

### 3. EVALUATION OF INERTIAL SUBRANGE SPECTRAL CONSTANTS

According to Kolmogorov's law for the inertial subrange the one-dimensional  $u$  spectrum can be expressed as

$$F_u(\kappa_1) = \alpha_1 \epsilon^{2/3} \kappa_1^{-5/3}, \quad (2)$$

where  $\kappa_1$  is the wavenumber in the  $x$  direction ( $\kappa_1 = 2\pi n/U$  by Taylor's hypothesis),  $\epsilon$  is the dissipation rate and  $\alpha_1$  is a universal constant estimated from various experiments to be about 0.5.

The  $u$  spectra computed from the Kansas measurements are remarkably smooth and follow the  $-5/3$  power law with typical scatter no more than a few per cent, so in conjunction with  $\epsilon$  values they are useful for estimating  $\alpha_1$ . The values in Fig. 1 are based on direct and indirect measurements (from hot-wire data and  $\phi_e$  curve respectively) and average  $0.50 \pm 0.05$  (standard deviation). An earlier estimate based on a portion of this data was  $0.52 \pm 0.05$  (Wyngaard and Coté 1971). Another analysis based on hot-wire spectral levels and  $\epsilon$  values gives  $0.53 \pm 0.02$  (Wyngaard and Pao 1972).

As discussed in detail later, the inertial subrange  $v$  and  $w$  spectral levels are higher than the  $u$  spectral levels by the factor of  $\sqrt{3}$  predicted by isotropy. Average  $\alpha_1$  estimates from  $v$  and  $w$  spectra are  $0.48 \pm 0.05$  and  $0.50 \pm 0.05$  respectively. Other recent experiments by Boston (1970) indicate a value of 0.51 for  $\alpha_1$  while Paquin and Pérold (1971) report 0.57. An unusually high value of 0.69 was observed by Gibson, Stegen and Williams (1970).

For temperature, Corrsin (1951) has proposed the following inertial subrange form:

$$F_\theta(\kappa_1) = \beta_1 \epsilon^{-1/3} N \kappa_1^{-5/3}, \quad (3)$$

where  $\beta_1$  is a constant analogous to  $\alpha_1$  in (1) and  $N$  is the dissipation rate of  $\overline{\theta^2}/2$ . We did not measure  $N$  directly, but the temperature variance budget (Wyngaard and Coté 1971) indicates that to a good approximation  $N$  is equal to the production rate, or  $-\overline{w\theta}(d\theta/dz)$ . This approximation leads to  $\beta_1$  estimates shown in Fig. 1, which average  $0.82 \pm 0.08$ . They agree well with our earlier estimate, based on a portion of the data, of  $0.79 \pm 0.10$  (Wyngaard and Coté 1971).

Unfortunately, there are two current conventions for the temperature variance dissipation rate in Eq. (3), and this causes confusion when  $\beta_1$  estimates from different experiments are compared. For symmetry with velocity we use the rate of destruction of  $\overline{\theta^2}/2$ ,

\*Spectra of all three velocity components are corrected for spatial averaging in the sonic anemometer (Kaimal et al. 1968). These effects are important only for  $\kappa_1 > 1/l$  where  $l$  (the sonic path length) is 0.2 m, but they restore the  $-5/3$  slope at the high end of the spectral bandwidth.

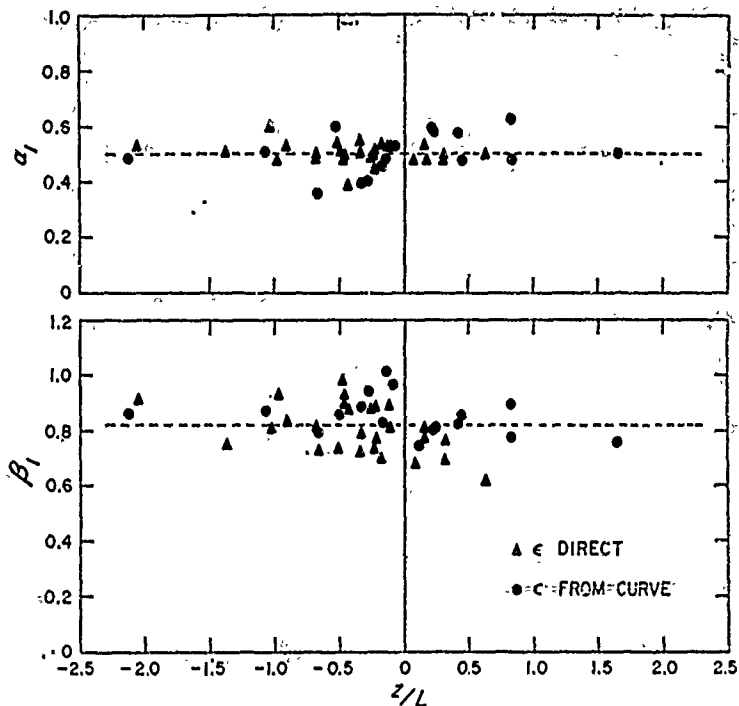


Figure 1. Spectral constants  $\alpha_1$  and  $\beta_1$  plotted against  $z/L$ . Direct  $\epsilon$  estimates are obtained from hot-wire measurements and indirect  $\epsilon$  estimates from the  $\phi_\epsilon$  curve in Fig. 2.

calling it  $N$ . Other workers use  $\chi$ , the rate of destruction of  $\bar{\theta}^2$ , and this leads to a factor of 2 difference in  $\beta_1$  values.

Recent  $\beta_1$  estimates, as defined in Eq. (3), show considerable spread. Panofsky's survey (1969) of Russian values shows a range from 0.41 to 0.88. Gibson and Schwarz (1963) measured 0.7 in the laboratory and Grant, Hughes, Vogel and Moilliet (1968) found 0.62 in the ocean. More recently Paquin and Pond (1971) obtained a value 0.83. Two other sets of estimates by Gibson *et al.* (1970) and Boston (1970), based on direct measurements of  $N$ , indicate  $\beta_1$  values of 2.3 and 1.6 respectively. At this point it is not clear why the spread in  $\beta_1$  values is so large.

#### 4. SPECTRA OF VELOCITY COMPONENTS

In recent years various efforts have been made to bring together velocity spectra from many sites, heights and thermal stabilities (e.g. Lumley and Panofsky 1964; Berman 1965; Busch and Panofsky 1968) and to define their general behaviour in terms of similarity parameters. A number of spectral forms have been suggested, all of which provide a reasonably good fit under near-neutral conditions. Our approach here will be somewhat different: we first collapse all spectra into universal curves in the inertial subrange and then observe the spectral behaviour at lower frequencies as a function of  $z/L$ .

We note from Eqs. (1) and (2) that the inertial subrange logarithmic  $u$  spectrum normalized with  $u_*^2$  has the form

$$\frac{nS_u(n)}{u_*^2} = \frac{\alpha_1}{(2\pi k)^{2/3}} \left( \frac{kz\epsilon}{u_*^3} \right)^{2/3} \left( \frac{nz}{U} \right)^{-2/3} \quad (4)$$

Using the definitions of  $f$  and  $\phi_\epsilon$ , this is

$$\frac{nS_u(n)}{u_*^2} = \frac{\alpha_1}{(2\pi k)^{2/3}} \phi_\epsilon^{2/3} f^{-2/3} \quad (5)$$

At  $f = 4$ , for example, and for  $k = 0.35^*$  and  $\alpha_1 = 0.5$ , Eq. (5) becomes

$$\left[ \frac{nS_u(\eta)}{u_*^2} \right]_{f=4} = 0.12 \phi_*^{2/3}. \quad (6)$$

The Kansas results have given the following interpolation formula for  $\phi_*$ , based on hot-wire measurements of  $\epsilon$ :

$$\phi_*^{2/3} = \begin{cases} 1 + 0.5|z/L|^{2/3}, & -2 \leq z/L \leq 0 \\ 1 + 2.5|z/L|^{3/5}, & 0 \leq z/L \leq +2 \end{cases}. \quad (7)$$

The inertial-subrange  $u$  spectral levels at  $f = 4$  predicted from Eqs. (6) and (7) are compared with the observed levels in Fig. 2. The agreement is good, with a standard deviation of about 10 per cent. Similar agreement is found between the  $0.16 \phi_*^{2/3}$  curve† and observed spectral levels for  $v$  and  $w$  at  $f = 4$ .

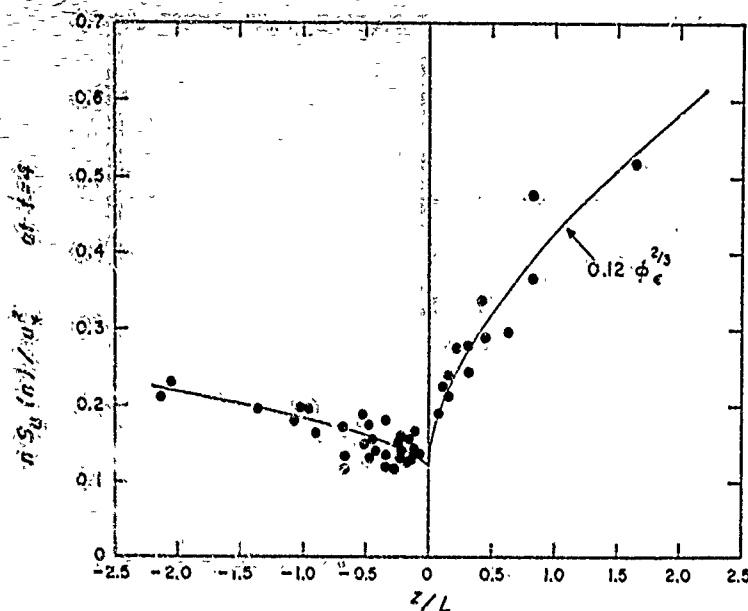


Figure 2. Normalized logarithmic  $u$  spectral estimates at  $f = 4$  compared with  $0.12 \phi_*^{2/3}$  curve derived from hot-wire data.

If we now include  $\phi_*^{2/3}$  in the normalization of  $u$ ,  $v$  and  $w$  spectra we remove the  $z/L$  dependence in their equations. This brings all spectra, regardless of  $z/L$ , into coincidence in the inertial subrange.

Starting with the  $w$  spectrum, we have the new form

$$\frac{nS_w(\eta)}{u_*^2 \phi_*^{2/3}} = 0.4 f^{-2/3}. \quad (8)$$

A plot of logarithmic  $w$  spectra normalized in this manner is shown in Fig. 3. The spectra converge to a  $-2/3$  line at the high-frequency end, but at lower frequencies there is a clearly established separation according to  $z/L$ . The apparent smoothness of the spectral plots and the clear demarcation between different categories of  $z/L$  permit one to draw isopleths corresponding to spectra at discrete values of  $z/L$ . We thus obtained a family of curves representing  $w$  spectra in the range  $+2 \geq z/L \geq -2$ . The curves, seen in Fig. 4,

\* Value of  $k$  obtained from Kansas data (Bastinger et al. 1971) and used in computing  $\phi_*$ . The conventional value for  $k$  is 0.4.

† Larger than Eq. (6) by a factor of  $4/3$  because of isotropy.

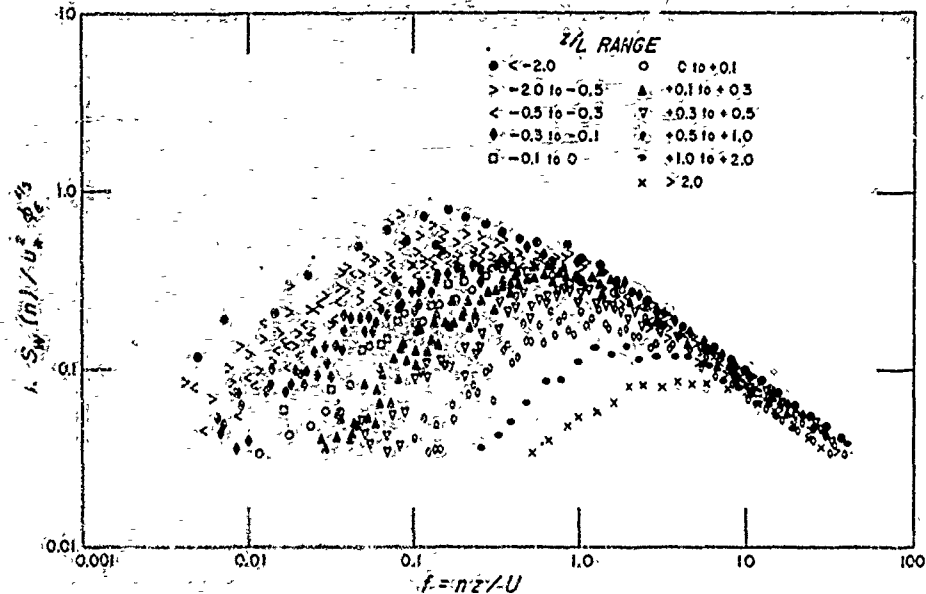


Figure 3. Normalized logarithmic  $w$  spectra, plotted against  $f$ , show low-frequency end separating according to  $z/L$ .

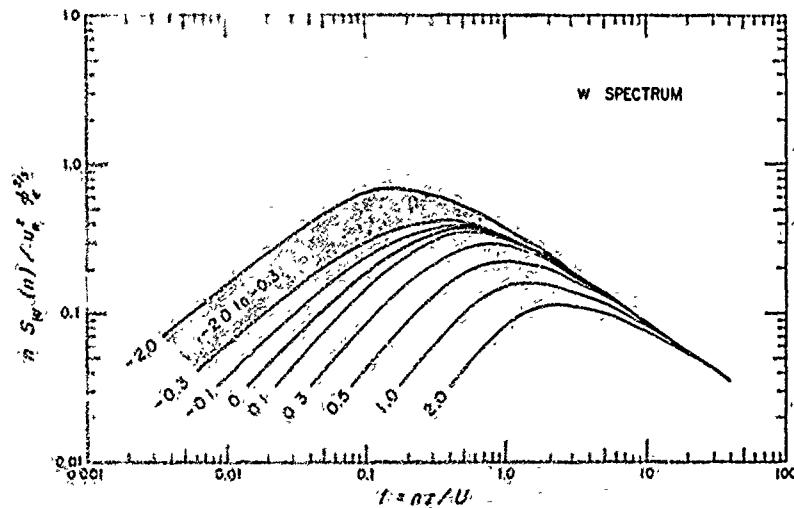


Figure 4. Generalized  $w$  spectrum for  $z/L$  values ranging from  $+2.0$  to  $-2.0$ . Stippling indicates absence of any well defined trend with  $z/L$ .

suggest an orderly progression of both the spectral peak and the low- $f$ /frequency roll-off in the direction of increasingly smaller  $f$  as  $z/L$  varies from  $+2.0$  to  $-0.3$ . In the range  $-0.3 > z/L > -2.0$ , however, the spectra are not arranged according to  $z/L$ , but tend to cluster in a random fashion within the stippled area.

Generalized spectral curves for  $u$  and  $v$  derived from plots similar to Fig. 3 are shown in Fig. 5 and 6. For  $z/L > 0$ ,  $u$  and  $v$  curves both display much the same shape and behaviour as  $w$ . The systematic progression with  $z/L$  observed on the stable side breaks down as  $z/L$  changes sign and becomes negative; the unstable spectra are confined to the stippled area with no particular regard to  $z/L$ .

An interesting feature of Figs. 5 and 6 is the separation between the areas occupied by

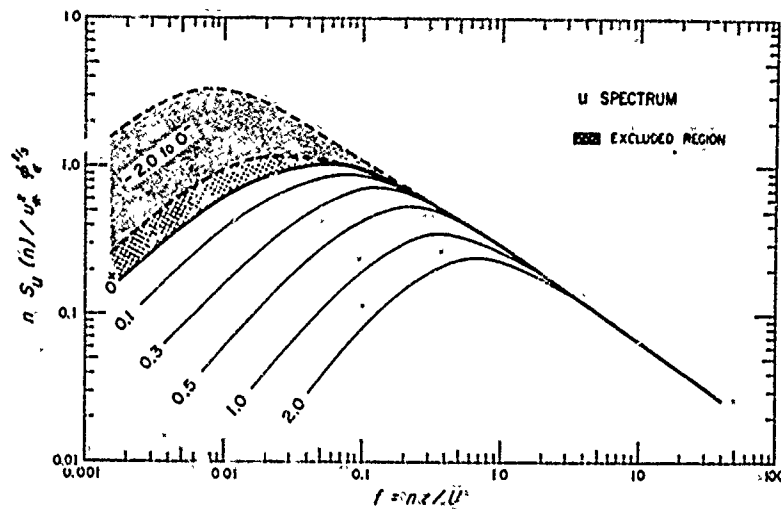


Figure 5. Generalized  $u$  spectrum for  $z/L$  values ranging from  $+2.0$  to  $-2.0$ .  $0^+$  and  $0^-$  denote  $z/L = 0$  approached from positive and negative sides respectively.

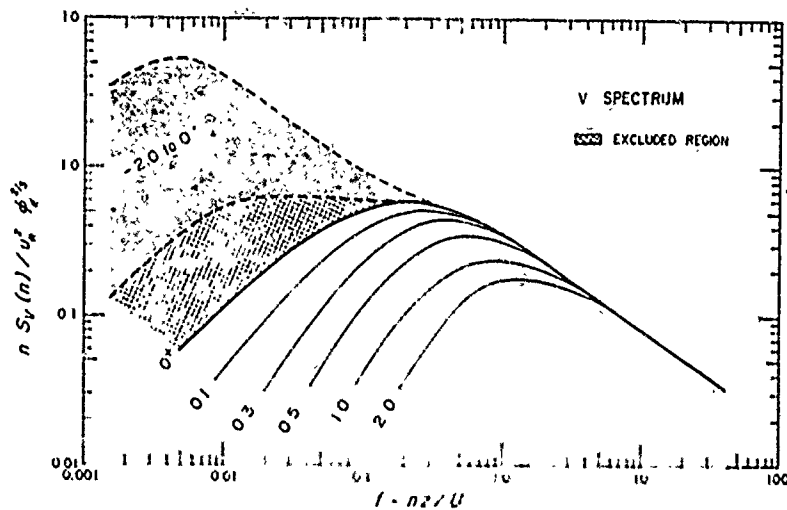


Figure 6. Generalized  $v$  spectrum for  $z/L$  values ranging from  $+2.0$  to  $-2.0$ .

the stable and unstable spectra\*. It appears as though the spectra are excluded from this region (indicated in these Figures by cross-hatch) and that a sudden shift in the predominant scales of motion occurs as  $z/L$  changes sign. Longitudinal vortex rolls, plumes and other convective circulations triggered by thermal instability have a profound effect on the scale of turbulence, but the abruptness with which the atmosphere responds to a change of sign in the potential temperature gradient remains surprising. The excluded region in  $f$  is approximately an octave wide in the  $u$  spectral plot and about a decade wide in the  $v$  plot. The heavy curve designated  $0^+$  in the figures defines the neutral limit for spectra on the stable side. The corresponding limit,  $0^-$ , on the unstable side is not uniquely defined and does not coincide with either of the two envelopes indicated by dashed curves.

Examination of the unstable  $v$  spectrum reveals two distinct régimes, one in the range  $f \geq 0.2$  where it follows closely the shape of the neutral spectrum, including the curvature

\*The same behaviour has been reported by Dr. Niels E. Busch (private communication) in  $v$  spectra obtained at 3.66 m during our 1968 Kansas experiments.



near its maximum, and another in the range  $f < 0.2$  dominated by a larger peak in the range  $0.005 < f < 0.02$ . These two régimes exist also in the unstable  $u$  spectrum, although they are not as clearly differentiated as in  $v$ . A change in spectral slope at  $f \approx 0.2$  marks the separation in the generalized  $u$  plot. More discussion on the behaviour of the horizontal velocity spectra follows in Section 8.

Comparing Figs. 4, 5 and 6 with spectra reported by other investigators we find good agreement with most measurements made in the first 100 m. Fig. 7 shows examples of some unstable spectra superimposed on the envelopes defined by the Kansas data. The individual data points shown are spectral estimates obtained over a tidal flat by Miyake, Stewart and Burling (1970). Spectra of  $u$  and  $w$  for Hanford, Round Hill, Cedar Hill and Vancouver are the composite curves published by Busch and Panofsky (1968). The  $v$  spectra for Hanford and Round Hill are from data reported by Elderkin (1966) and Cramer and Record (1969) respectively.

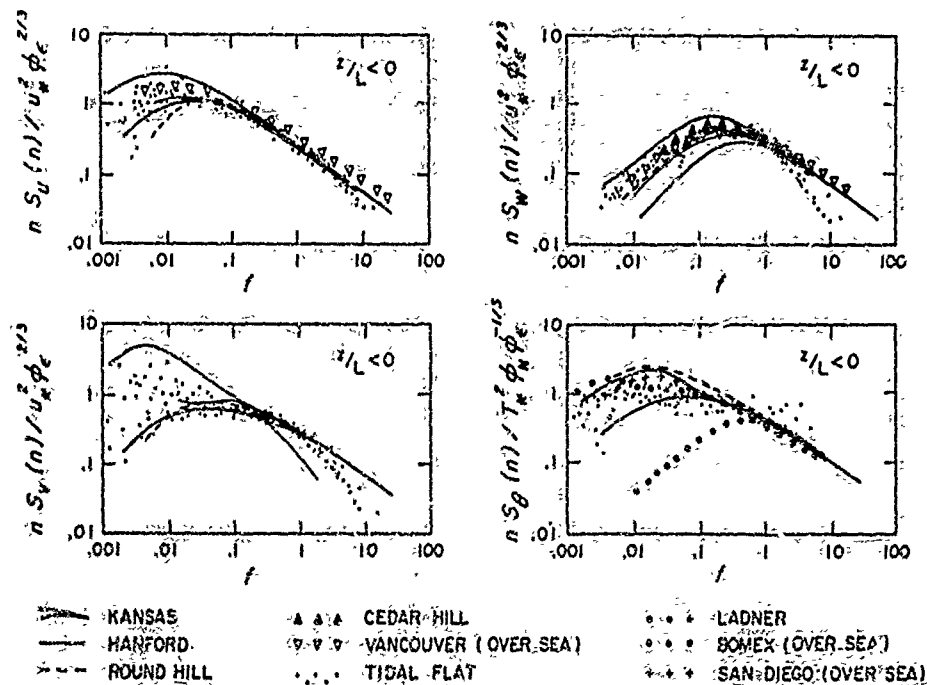


Figure 7. Envelopes for the unstable Kansas spectra compared with other recent spectra.

Spectral estimates for the tidal flat roll off more steeply at the high-frequency end than other spectra, but this discrepancy is removed when the estimates are corrected for spatial response in the sonic anemometer array. At lower frequencies the tidal flat spectra fit the Kansas data remarkably well. The severe high-frequency attenuation of the Hanford  $v$  spectrum is probably related to the time lag of the servo system which hunts the azimuth wind direction. The Vancouver spectra of  $u$  and  $w$ , derived from measurements over the sea by Weller and Burling (1967), appear to have slightly higher inertial-subrange intensities than the other spectra.

##### 5. SPECTRUM OF TEMPERATURE

The inertial subrange temperature spectrum may also be expressed in nondimensional form by rearranging terms in Eq. (3). The resulting expression is

$$\frac{nS_\theta(n)}{T_*^2} = \frac{\beta_1}{(2\pi k)^{2/3}} \phi_N \phi_e^{-1/3} f^{-2/3}, \quad (9)$$

where  $T_*$  is the scaling temperature and  $\phi_N$  and  $\phi_e$  are the dimensionless dissipation rates for  $\bar{\theta}^2/2$  and turbulent energy respectively. The observed balance between the production and dissipation rates (i.e.  $N = -w\bar{\theta} d\theta/dz$ ) enables us to substitute  $\phi_h$  for  $\phi_N$ . An empirical relationship for  $\phi_h$  has been derived from the Kansas data by Businger *et al.* (1971).

$$\phi_h = \begin{cases} 0.74(1 - 9z/L)^{-1/2}, & -2 \leq z/L \leq 0 \\ 0.74 + 4.7z/L, & 0 \leq z/L \leq +2 \end{cases} \quad (10)$$

Since the product  $\phi_N \phi_e^{-1/3}$  is a function only of  $z/L$ , the expression in Eq. (9) is consistent with similarity theory. At  $f = 4$  and using  $\beta_1 = 0.8$  and  $k = 0.35$ , Eq. (9) becomes

$$\left[ \frac{nS_\theta(n)}{T_*^2} \right]_{f=4} = 0.19 \phi_h \phi_e^{-1/3}. \quad (11)$$

The prediction in Eq. (11) is compared with observation in Fig. 8. The agreement is good, with a standard deviation of no more than 10 per cent. A roughly similar curve was obtained earlier by Panofsky (1969). Allowing for the difference in the selected  $f$  value and the use of  $k$  in the definition of  $T_*$ , both curves show intercepts at  $z/L = 0$  which agree within 10 per cent.

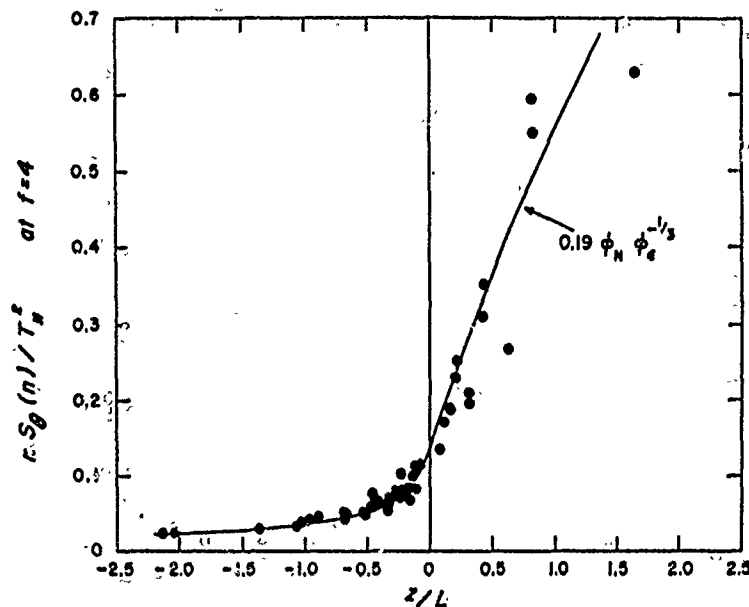


Figure 8. Normalized logarithmic  $\theta$  spectral estimates at  $f = 4$  compared with  $0.19 \phi_N \phi_e^{-1/3}$  curve derived from hot-wire and mean profile data.

By including  $\phi_N \phi_e^{-1/3}$  in the normalization of the logarithmic temperature spectrum we collapse all inertial subrange spectra into a single curve (see Fig. 9). The stable temperature spectra, like those of velocity, separate into distinct categories of  $z/L$  while all the unstable spectra crowd into the relatively narrow band indicated by the stippled area. Even though regions occupied by the stable and unstable spectra appear contiguous, the transition from one to the other is not smooth. The spectrum shifts from  $0^+$  to the outer edge of the stippled area as  $z/L$  changes from positive to negative; with increasingly negative  $z/L$  the spectrum moves back towards  $0^+$ . The trend is reversed when  $z/L$  moves in the opposite direction, from negative to positive.

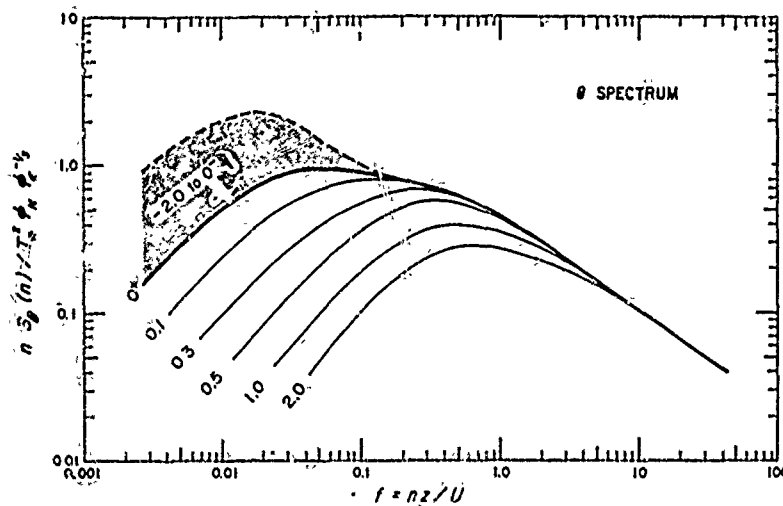


Figure 9. Generalized  $\theta$  spectrum for  $z/L$  values ranging from  $+2.0$  to  $-2.0$ .

The progressive shift in the  $\theta$  spectrum within the stippled area is partly a consequence of using  $T_*^2$  for normalization ( $\sigma_\theta/T_*$  has a cusp-like behaviour near neutral, Wyngaard, Côté and Izumi (1971)), but the tendency of the logarithmic spectral peak to shift towards increasingly larger  $f$  with increasing instability is real. Lumley and Panofsky (1964) have pointed out that the location of the  $\theta$  spectral peak intermediate between those of  $u$  and  $w$  suggests that the fluctuations in both velocity components contribute to fluctuations in  $\theta$ . Extending this argument further, one could interpret the shift in the logarithmic  $\theta$  spectral peak to larger values of  $f$  as being the result of a shift in the relative influence of  $u$  and  $w$  on  $\theta$ . As the surface layer becomes increasingly unstable, the influence of  $w$  grows steadily, while that of  $u$  declines. This shift is reflected in the trend of the correlation coefficients listed in Table 2.

TABLE 2. MEAN CORRELATION COEFFICIENT FOR DIFFERENT CATEGORIES OF  $z/L$ . THE TIME SERIES WERE HIGH-PASS FILTERED BY DIFFERENCING WITH RESPECT TO A 5-MIN MOVING AVERAGE

$-z/L$	0 - 0.1	0.1 - 0.3	0.3 - 0.5	0.5 - 1.0	1.0 - 2.0
$\gamma_{\theta}$	-0.56	-0.41	-0.33	-0.22	-0.18
$\gamma_{u\theta}$	+0.37	+0.44	+0.50	+0.54	+0.59
$\gamma_{w\theta}$	-0.31	-0.27	-0.22	-0.19	-0.14

The generalized curves in Fig. 9 agree well with most spectra obtained in recent years (see Fig. 7). Conversion of spectra from other sources into the format of Fig. 7 was based on the observed  $\phi_N \phi_t^{-1/2}$  behaviour in Kansas. An exception is made with the Bomex data for which  $\phi_N$  appears to be five to six times larger than for Kansas or other sites, but show  $\beta_1$  values virtually identical to those from Kansas. Here the inertial subrange fit was determined on the basis of  $\beta_1$  values reported by Paquin and Pond (1971).

Spectral estimates for the tidal flat (Miyake *et al.* 1970) show fair agreement with the Kansas spectra at  $f < 1.0$ , but depart markedly at  $f > 1.0$ , presumably due to noise contamination inherent in (their) sonic temperature signals. Spectra from the other sources follow the generalized inertial subrange behaviour quite well. The composite curve for Round Hill (Panofsky 1969) does not show the flatness at  $f \approx 0.1$  seen in the Kansas spectra, but those for Ladner (McBean 1970) and San Diego (Phelps and Pond 1971) show this

clearly. The curve for Bomex (McBean 1970; Phelps and Pond 1971) stands out in sharp contrast to other spectra; its peak is shifted to a higher value of  $f$  ( $\approx 0.8$ ) and the spectral intensities on the low-frequency side are much lower. The Bomex curve, in fact, resembles the stable spectrum at  $z/L = +0.5$  in the generalized plot of Fig. 9, although conditions during the Bomex runs are reported as unstable ( $-0.33 < z/L < -0.11$ ). The reasons for such anomalous behaviour in the Bomex data are still unclear.

## 6. COSPECTRA OF REYNOLDS STRESS AND HEAT FLUX

In this Section we will examine the behaviour of the three non-zero cospectra in the surface layer:  $uw$ ,  $w\theta$  and  $u\theta$ . These are essentially the cospectra of the shearing stress; vertical heat flux and horizontal heat flux. The cospectrum is inherently more difficult to measure than the power spectrum because the correlations between the variables being compared are sometimes very small. The cospectra are also particularly sensitive to instrumental errors which introduce 'cross-talk' between the two variables. For example, instrument levelling and alignment errors (Kaimal and Haugen 1969) cause cross-talk between  $u$  and  $w$ , while a sonic temperature signal has  $u$ -contamination (Kaimal 1969). At high wave numbers, cospectral distortion can also arise from spatial averaging in the sensor and from separation distance between sensors. To avoid such distortion we have limited our  $\kappa_1$  to less than  $1/l$ , where  $l$  (the sonic path length) is 0.2 m. The smallest wavelength resolved is then 1.25 m. In analysing our cospectra we adopt the same approach used with spectra, namely, to collapse all the curves into a single universal curve at large  $f$ . The functional relationship between the normalized cospectral intensities at  $f = 4$  and  $z/L$  are determined from plots similar to Figs. 2 and 8.

The cospectra of  $uw$  and  $w\theta$  show a  $-7/3$  power law in the inertial subrange. The dimensional arguments for such a power law and the experimental verification of it from the Kansas data are presented by Wyngaard and Coté (1972) in a companion paper in this issue. Other investigators (Panofsky and Mares 1968; Kukharets and Tsvang 1969) have reported a  $-8/3$  cospectral slope but the more recent measurements of McBean (1970) appear to favour the  $-7/3$  slope.

Cospectra of  $u\theta$  are rare in the literature. The few examples presented by Sitaraman (1970) are limited in bandwidth ( $f < 1.0$ ) and do not, therefore, provide any information about the inertial subrange behaviour of  $u\theta$ . Our data show an average slope of  $-5/2$  in the range  $1 < f < 10$ . No dimensional justification can be made for this power law, but it serves the present purpose of collapsing the cospectra into a single curve.

### (a) $uw$ cospectrum

In the  $-7/3$  region the normalized logarithmic  $uw$  cospectrum should be a function only of  $z/L$  and  $f$ . Denoting the  $z/L$  dependence by a function  $G$ , we can write

$$-\frac{n C_{uw}(n)}{u_*^2} \propto G(z/L) f^{-4/3},$$

where  $C_{uw}(n)$  is the cospectral density. The function  $G(z/L)$  determined empirically from cospectral estimates evaluated at  $f = 4$  (see Fig. 10) has the form

$$G(z/L) = \begin{cases} 1, & -2 \leq z/L \leq 0 \\ 1 + 7.9 z/L, & 0 \leq z/L \leq +2 \end{cases} \quad (12)$$

To bring the stress cospectra into coincidence in the  $-7/3$  region ( $-4/3$  for the logarithmic cospectrum) we divide by  $G(z/L)$

$$-\frac{n C_{uw}(n)}{u_*^2 G(z/L)} = \frac{0.56}{(2\pi)^{4/3}} f^{-4/3}. \quad (13)$$

As with spectra described in earlier Sections, the normalization in Eq. (13) separates the

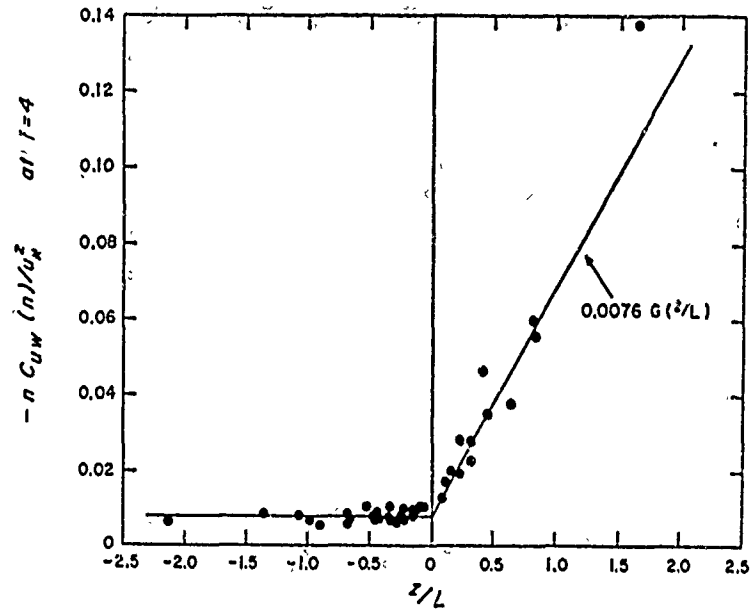


Figure 10. Normalized logarithmic  $uw$  cospectral estimates at  $f = 4$  compared with empirical formula in Eq. (12),

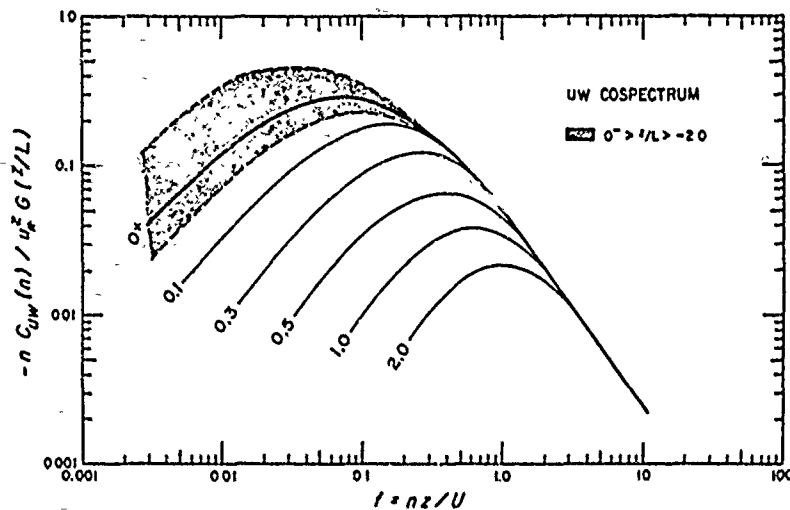


Figure 11. Generalized  $uw$  cospectrum for  $z/L$  values ranging from  $+2.0$  to  $-2.0$ .

stress cospectra into clearly defined categories of  $z/L$  (see Fig. 11). The position of the stable cospectrum shifts as a function of  $z/L$ , while all the unstable cospectra crowd into a narrow band indicated in Fig. 11 by the stippled area. The dashed curves approximate the upper and lower limits of scatter in the unstable cospectral estimates. There is some overlap between the stable and unstable regions,  $0^+$  being located within the stippled area. This overlap is consistent with the constraint imposed by our normalization, which requires the integral of the  $uw$  cospectrum for  $z/L \leq 0$  to be unity.

The logarithmic cospectral peak is spread over only two decades of  $f$ , separated roughly as follows: between 0.01 and 0.1 for  $z/L < 0$  and between 0.1 and 1.0 for  $z/L > 0$ . At very low frequencies ( $f < 0.01$ ), particularly at the 22.6 m level, the cospectral estimates

show a tendency to reverse sign and become positive. Similar behaviour has been reported by Zubkovsky and Koprov (1969) and McBean (1970). In the Kansas data this sign reversal is observed only under unstable conditions when the low frequency cospectral estimates fluctuate between large positive and negative values. This erratic behaviour in the cospectrum occurs precisely in the frequency range where the logarithmic spectra of  $u$  and  $v$  attain their maxima, i.e., the range where the effects of surface layer convective circulations are most strongly felt. Some convective elements have been found to transport momentum upward, against the velocity gradient (Kaimal and Businger 1970), others to transport it downward (Haugen *et al.* 1971). It is not surprising, therefore, that cospectral estimates in this range are erratic and highly unpredictable.

Local free convection arguments (Wyngaard and Coté 1972) predict that  $G(z/L)$  should be constant under very unstable conditions, and as with other similar predictions (Wyngaard *et al.* 1971) it is found that this behaviour holds right up to  $z/L = 0$ . Under unstable conditions, therefore, the inertial subrange stress cospectral level is determined solely by  $u_*^2$  and  $f$ .

In Fig. 14, the unstable stress cospectra from Kansas are compared with results obtained by other investigators. The cospectral estimates from Ladner (McBean 1970) agree well with the Kansas data while those from Bomex, described in the same reference, appear higher by a factor of 1.5 at  $f > 1.0$ . The composite cospectrum for Round Hill (Panofsky and Mares 1968) falls off more sharply at  $f > 1.0$ , but otherwise shows fair agreement with our results. The composite curves for Hanford and Vancouver (also from Panofsky and Mares 1968) show even greater departure in the inertial subrange, with slopes and cospectral intensities substantially different from any observed in Kansas.

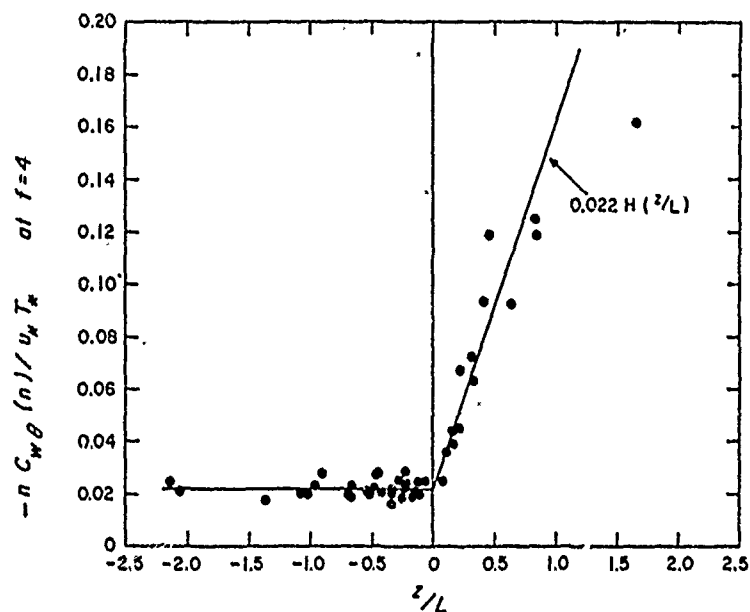


Figure 12. Normalized logarithmic  $w\theta$  cospectral estimates at  $f = 4$  compared with empirical formula in Eq. (14).

(b)  $w\theta$  cospectrum

Applying the same arguments used for the  $uw$  cospectrum but denoting the  $z/L$  dependence by a different function,  $H$ , we write

$$-\frac{n C_{w\theta}(n)}{u_* T_*} \propto H(z/L) f^{-4/3}.$$

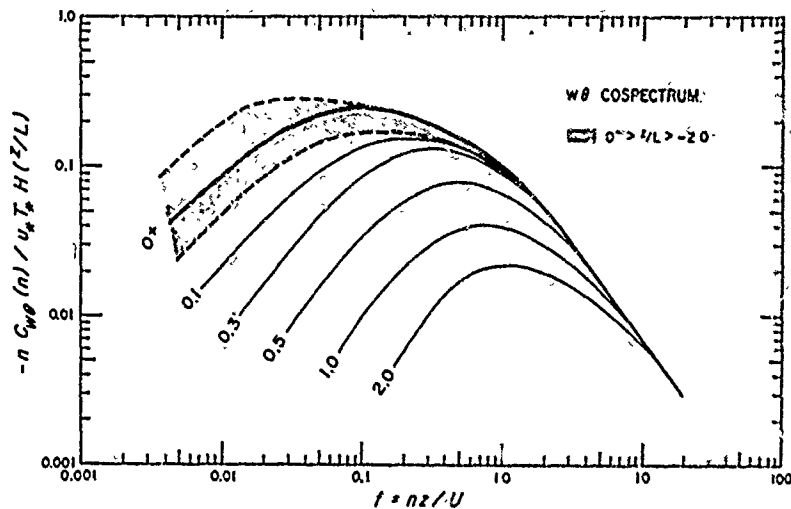


Figure 13. Generalized  $w\theta$  cospectrum for  $z/L$  values ranging from  $+2.0$  to  $-2.0$ .

$H(z/L)$  determined from the cospectral values evaluated at  $f = 4$  (see Fig. 12) has the form

$$H(z/L) = \begin{cases} 1, & -2 \leq z/L \leq 0 \\ 1 + 6.4 z/L, & 0 \leq z/L \leq +2 \end{cases} \quad (14)$$

The negative sign in the proportionality results from the definition of  $T_*$ ;  $u_* T_*$  is, therefore, the negative vertical heat flux. The constancy of  $H(z/L)$  under unstable conditions is consistent with local free convection behaviour.

To bring the  $w\theta$  cospectra into coincidence in the  $-4/3$  region we divide by  $H(z/L)$ .

$$-\frac{n C_{w\theta}(n)}{u_* T_* H(z/L)} = \frac{1.62}{(2\pi)^{4/3}} f^{-4/3} \quad (15)$$

The cospectrum thus normalized (see Fig. 13) shows behaviour very similar to the stress cospectrum, both in regard to the location of its peak and the roll-off on the low-frequency side. But on the high-frequency side, the  $-4/3$  line is shifted at least an octave higher on the frequency scale. This extended contribution at the high-frequency end gives the  $w\theta$  cospectra, especially the unstable ones, a flatter appearance in the midrange. As in Eq. (13), this normalization requires the integral of the cospectrum for  $z/L \leq 0$  to be unity, causing the  $0^+$  curve to lie within the stippled area. The inertial subrange cospectral level for  $w\theta$  is about three times as large as for  $uw$ . Smaller eddies, therefore, transport heat more effectively than momentum. The ratio of the two cospectra in the inertial subrange can be expressed as

$$\frac{C_{w\theta}(n)}{C_{uw}(n)} = 2.9 \frac{H(z/L) T_*}{G(z/L) u_*} \approx 2.9 (\overline{w\theta}/\overline{uw}), \quad -2 \leq z/L \leq +2. \quad (16)$$

Since the integral of the cospectrum is the covariance, Eq. (16) has the corollary that the larger eddies ( $f < 1.0$ ) transport heat less effectively than momentum.

The agreement between the  $w\theta$  cospectra obtained by McBean (1970) at Ladner and the Kansas results of Fig. 13 is extremely good. However, his BOMEX data show considerable departure; the bandwidth is narrower and the logarithmic cospectral peak is shifted about a decade higher than in results obtained over land. A comparison of the unstable runs from Ladner and BOMEX with the Kansas curves is given in Fig. 14. The average Round Hill cospectrum (Panofsky and Mares 1966) also indicated in the Figure, falls off more rapidly, starting at least an octave lower than the Kansas cospectrum.

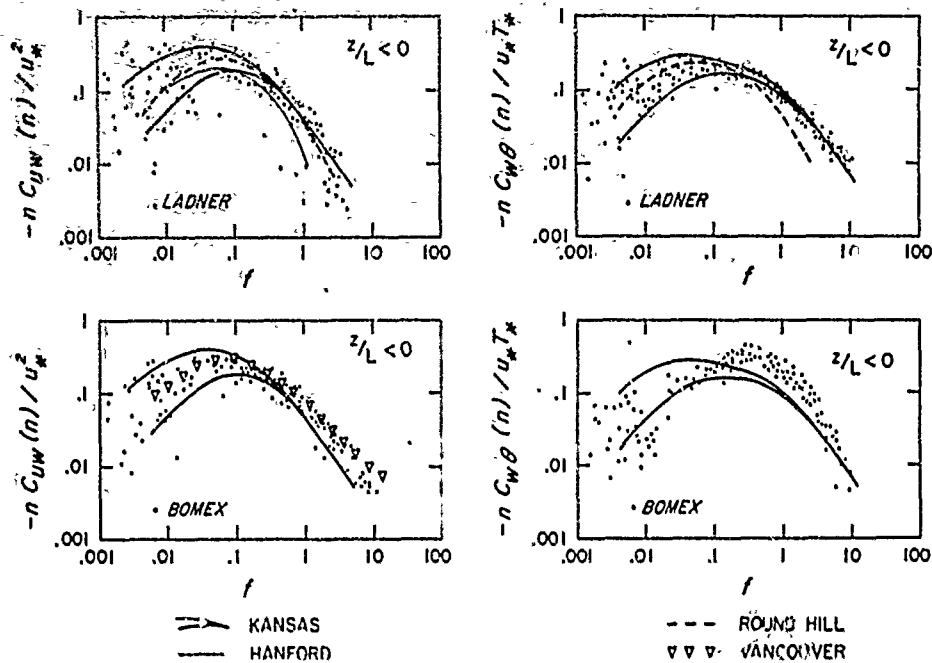


Figure 14. Envelopes for unstable Kansas cospectra compared with other recent cospectra.

(c)  $u\theta$  cospectrum

The  $-5/2$  cospectral slope ( $-3/2$  for the logarithmic cospectrum) indicated for  $u\theta$  is not as clearly established as are the  $-7/3$  slopes for  $uw$  and  $w\theta$ . The stable runs show a slope of  $-5/2$  at all heights but the unstable runs show slopes varying from  $-3$  (at 5.66 m), to  $-7/3$  (at 22.6 m). The theoretical prediction of  $-3$  by Wyngaard and Coté (1972) is approached only in a few cases at the lowest height.

Using the overall average of  $-5/2$  for the cospectral slope we write

$$\frac{n C_{u\theta}(n)}{u_* T_*} \propto K(z/L) f^{-3/2}$$

where  $K(z/L)$  is a function determined empirically (see Fig. 15) to be

$$K(z/L) = \begin{cases} 1, & -2 \leq z/L \leq 0 \\ 1 + 17.4 z/L, & 0 \leq z/L \leq +2 \end{cases} \quad (17)$$

Like  $G(z/L)$  and  $H(z/L)$ , this function is also a constant under unstable conditions. As before, we collapse the logarithmic cospectra at the high-frequency end by including  $K(z/L)$  in the normalization.

$$\frac{n C_{u\theta}(n)}{u_* T_* K(z/L)} = \frac{0.55}{(2\pi)^{3/2}} f^{-3/2} \quad (18)$$

The normalized  $u\theta$  curves in Fig. 16 are spread over a much wider range of cospectral intensities than either  $uw$  or  $w\theta$ . The stable cospectra show the same systematic progression with  $z/L$  seen in earlier Figures. The overlap between the stable and unstable regions is larger than for  $uw$  and  $w\theta$ , apparently the result of using  $u_* T_*$  instead of  $\overline{u\theta}$  for normalization. For  $z/L < 0$  we can use the local free convection prediction of Wyngaard *et al.* (1971) and write

$$u_* T_* = \overline{u\theta} / 5 \phi_m \phi_h; \quad z/L < 0. \quad (19)$$

Although no attempt is made in Fig. 16 to show the trend within the unstable co-



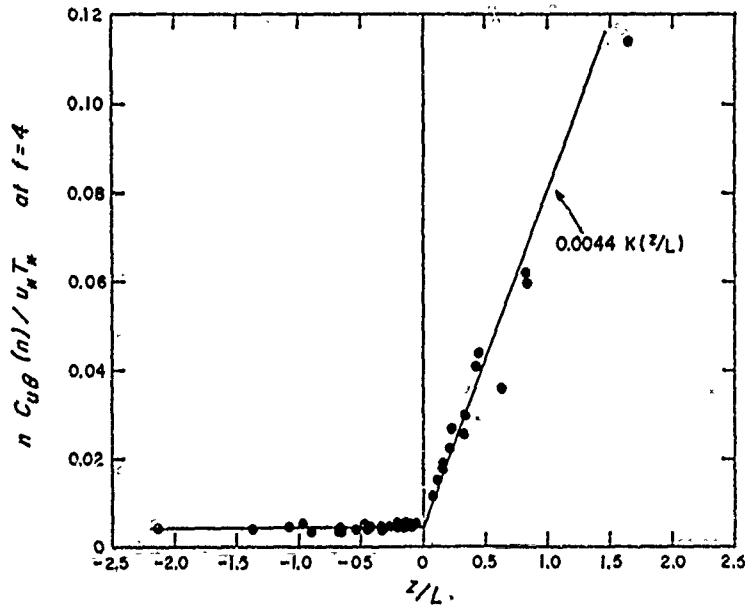


Figure 15. Normalized logarithmic  $u\theta$  cospectral estimates at  $f = 4$  compared with empirical formula in Eq. (17).

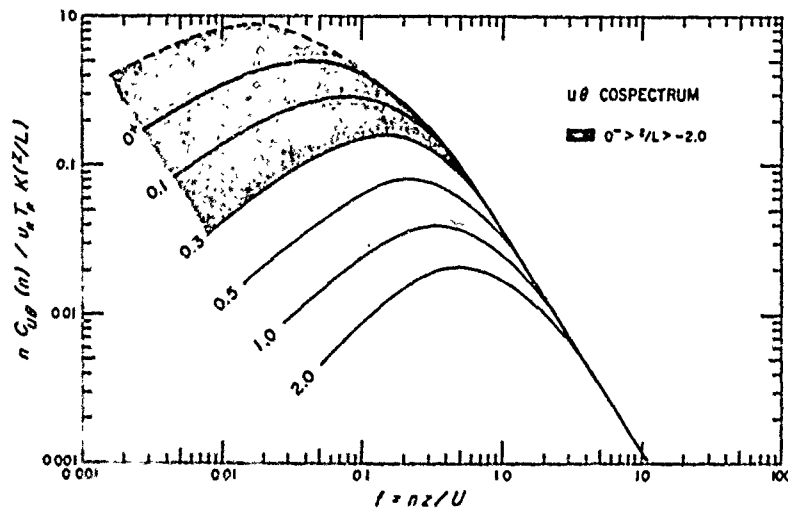


Figure 16. Generalized  $u\theta$  cospectrum for  $z/L$  values ranging from  $+2.0$  to  $-2.0$ .

spectra, there is nevertheless a rough separation according to  $z/L$ . The top third of the stippled area is occupied predominantly by cospectra in the  $z/L$  range  $0$  to  $-0.3$ , the middle third by the  $z/L$  range  $-0.3$  to  $-1.0$  and the lower third by the  $z/L$  range  $-1.0$  to  $-2.0$ .

The relative efficiency of the horizontal and vertical heat transports in the high-frequency end of the cospectrum can be estimated from Eq. (15) and (18)

$$\frac{C_{u\theta}(n)}{C_{w\theta}(n)} = - \frac{0.34}{(2\pi f)^{1/6}} \frac{K(z/L)}{H(z/L)} \quad (20)$$

At  $f = 1$ , the ratio varies from a  $-0.25$  (constant for  $z/L < 0$ ) to an asymptotic value of

-0.68 on the stable side. It is interesting to note that the ratio is considerably less than unity in the range  $f > 1.0$ , which suggests that the smaller eddies always transfer heat more effectively in the vertical than in the horizontal. The reverse is true with the larger eddies, this being most pronounced in stable conditions when  $u\theta$  cospectral levels become 2 - 3 times larger than the  $w\theta$  levels.

### 7. EMPIRICAL FORMULAS FOR NEUTRAL LAPSE RATE

The relationships derived in the previous Sections uniquely define, for all stabilities, the behaviour in the inertial subrange. At lower frequencies, empirical formulas can be obtained for specific ranges of  $z/L$ . To enable comparison with other atmospheric and laboratory data we present formulae which fit our neutral spectra and cospectra. For  $w$  the neutral spectrum is defined unambiguously as the curve separating the near-neutral stable and unstable spectra. For all other spectra and cospectra, where the transition is obscured by a gap or an overlap, the limiting curve on the stable side,  $0^+$ , is used instead.

It is quite apparent that there is considerable similarity in the shapes of the logarithmic spectra and cospectra. On the high frequency side they fall off according to  $-2/3$ ,  $-4/3$ , or  $-3/2$  depending on the parameter; on the low-frequency side the slope is very nearly  $+1.0$ . The empirical formulae, therefore, have roughly similar form.

At  $z/L = 0$ , where  $\phi_v = G = H = K = 1$  and  $\phi_h = 0.74$  we have

$$nS_u(n)/u_*^2 = 105 f/(1 + 33 f)^{5/3} \quad (21a)$$

$$nS_v(n)/u_*^2 = 17 f/(1 + 9.5 f)^{5/3} \quad (21b)$$

$$nS_w(n)/u_*^2 = 2 f/[1 + 5.3 (f)^{5/3}] \quad (21c)$$

$$nS_\theta(n)/T_*^2 = \begin{cases} 53.4 f/(1 + 24 f)^{5/3}, & f \leq 0.15 \\ 24.4 f/(1 + 12.5 f)^{5/3}, & f \geq 0.15 \end{cases} \quad (21d)$$

$$-nC_{uw}(n)/u_*^2 = 14 f/(1 + 9.6 f)^{2.4} \quad (21e)$$

$$-nC_{w\theta}(n)/u_* T_* = \begin{cases} 11 f/(1 + 13.3 f)^{1.75}, & f \leq 1.0 \\ 4.4 f/(1 + 3.8 f)^{2.4}, & f \geq 1.0 \end{cases} \quad (21f)$$

$$nC_{u\theta}(n)/u_* T_* = 40 f/(1 + 14 f)^{2.6} \quad (21g)$$

The above formulae are good approximations of the observed curves (see Fig. 17 for plots). The only departure exceeding  $\pm 10$  per cent are at the low-frequency ends of the  $u$  spectrum and the  $u\theta$  cospectrum. Empirical curves proposed by Busch and Panofsky (1968) and Panofsky and Mares (1968) are very similar to those shown in Fig. 17, except for a small displacement on the ordinate. Although our formulae for the cospectra indicate asymptotes which are steeper than the observed values, the equation fit the data extremely well in the range  $0.01 < f < 4.0$ .

### 8. BEHAVIOUR AT LOW FREQUENCIES

In earlier Sections of this paper frequent mention was made of systematic shifts in the spectral and cospectral peaks with respect to changes on  $z/L$ . The most consistent behaviour in the logarithmic peak frequency,  $f_m$ , is observed under stable conditions, i.e.,  $z/L > 0$ . For  $z/L < 0$  only the spectra of  $\theta$  and  $w$  show a systematic trend; the others have their peaks scattered over a decade or more of  $f$ .

Figs. 18 and 19 shows plots of  $f_m$  vs.  $z/L$  in the ranges where a clear relationship exists between them. The curves drawn through the data points are fitted by eye. Different symbols are used to identify the different heights of observation and they all apparently fit the same curve. In fact, on the stable side,  $f_m$  exhibits nearly the same trend with  $z/L$  for all parameters. The following approximations can be made for the stable spectral peaks:

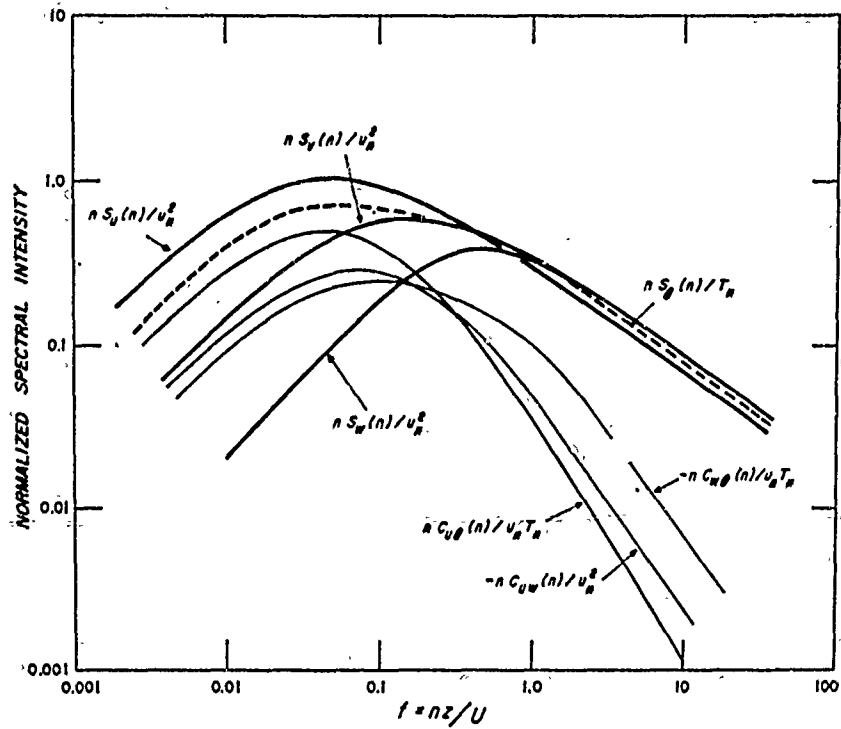


Figure 17. Empirical curves for spectra and cospectra for  $z/L = 0$  (see formulas in Section 7).

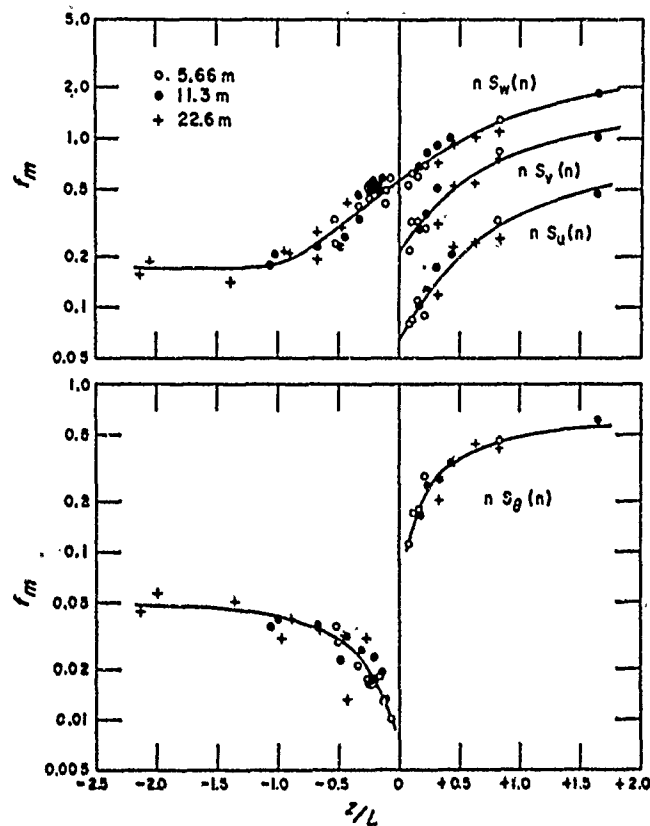
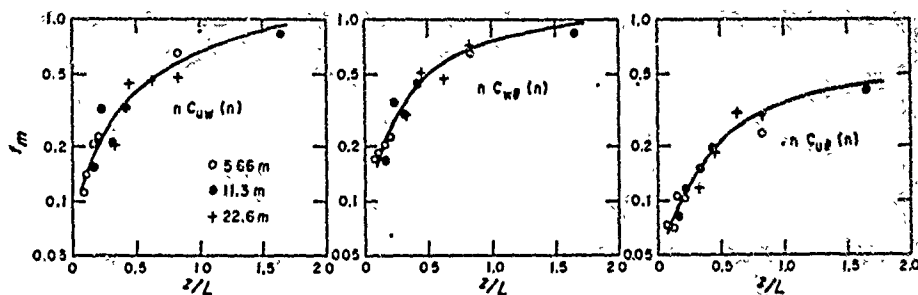


Figure 18. Logarithmic spectral peak for  $u, v, w$  and  $\theta$  plotted against  $z/L$ . Curves shown are fitted by eye.

Figure 19. Logarithmic spectral peaks for  $uw$ ,  $w\theta$  and  $u\theta$ .

$$(f_m)_w \approx 5(f_m)_u \approx 2(f_m)_v \approx 3 \cdot 3(f_m)_\theta \quad (22a)$$

$$(f_m)_{uw} \approx (f_m)_{w\theta} \approx 2(f_m)_{u\theta} \quad (22b)$$

On the unstable side,  $f_m$  for the  $w$  spectrum continues to decrease with decreasing  $z/L$ , but levels off to a constant value of about 0.17 when  $z/L$  exceeds  $-1.0$ . Spectra of  $w$  obtained from the Cedar Hill tower (Kaimal and Haugen 1967) show approximately the same value of  $f_m$  maintained to a height of 320 m.

Local free convection predictions, which are successful for other statistics of  $w$  and  $\theta$  (Wyngaard *et al.* 1971), should also hold for their  $f_m$  values. In local free convection  $L$  loses physical significance and  $z$  becomes the only important length scale, so that the peak wavelength  $(\lambda_m)_w$  for example, is proportional to  $z$ . It follows that

$$(f_m)_w = z/(\lambda_m)_w = \text{constant},$$

as observed.

The peak frequency of the unstable temperature spectrum shows the opposite trend from  $w$  in its approach to local free convection state. Proceeding from zero to increasingly negative values of  $z/L$ ,  $f_m$  increases from 0.01 to 0.05 in the range  $0 > z/L > -2.0$  and levels off to a constant value of about 0.05 at  $z/L = -2.0$ . The trend near  $z/L = 0$  suggests a discontinuity at neutral with a jump of approximately one decade at the transition. A similar plot presented by Panofsky (1969) using data from Round Hill shows greater scatter, but roughly the same behaviour as Fig. 18.

Peak frequencies of  $u$  and  $v$  also show discontinuity at  $z/L = 0$ , the shift being of the order of 1 to 2 decades. One obvious consequence of this discontinuity is the excluded region in the generalized spectral plots of Figs. 5 and 6. The absence of any clear dependence between  $f_m$  and  $z/L$  on the unstable side is attributed largely to the influence of mesoscale features in the atmosphere; in fact there is a tendency for  $n_m$ , rather than  $f_m$ , to be constant with height. The constancy of  $n_m$  with height fits in with recent observations (Kaimal and Businger 1970) which indicate that convective systems have vertical integrity so that the time intervals between them change little with height. For the unstable  $u$  and  $v$  spectra,  $n_m$  falls invariably between 0.003 and 0.005 Hz corresponding to time periods of 3 to 5 min, approximately the average interval between the large convective systems in the surface layer.

The strong similarity of shape among the stable spectra suggests that a different normalization might be appropriate. The normalizations used in the previous plots tended to exaggerate the separation between peaks of the stable spectra. This vertical separation is greatly reduced by dividing the logarithmic spectrum by the appropriate variance\* rather than by  $u_*^2$ . A modified frequency scale  $f/f_0$ , where  $f_0$  is the intercept of the extrapolated inertial subrange spectrum with the  $nS_\alpha(n)/\bar{\alpha}^2 = 1$  line ( $\alpha = u, v, w$  or  $\theta$ ), brings all spectra into coincidence on a  $-2/3$  line in the inertial subrange. When all stable spectra are plotted in this manner, they display a universal shape (see Fig. 20) which can be

\*Variance used here is limited to a bandwidth 0.005 to 10 Hz in order to avoid the influence of trends and long-term oscillations.

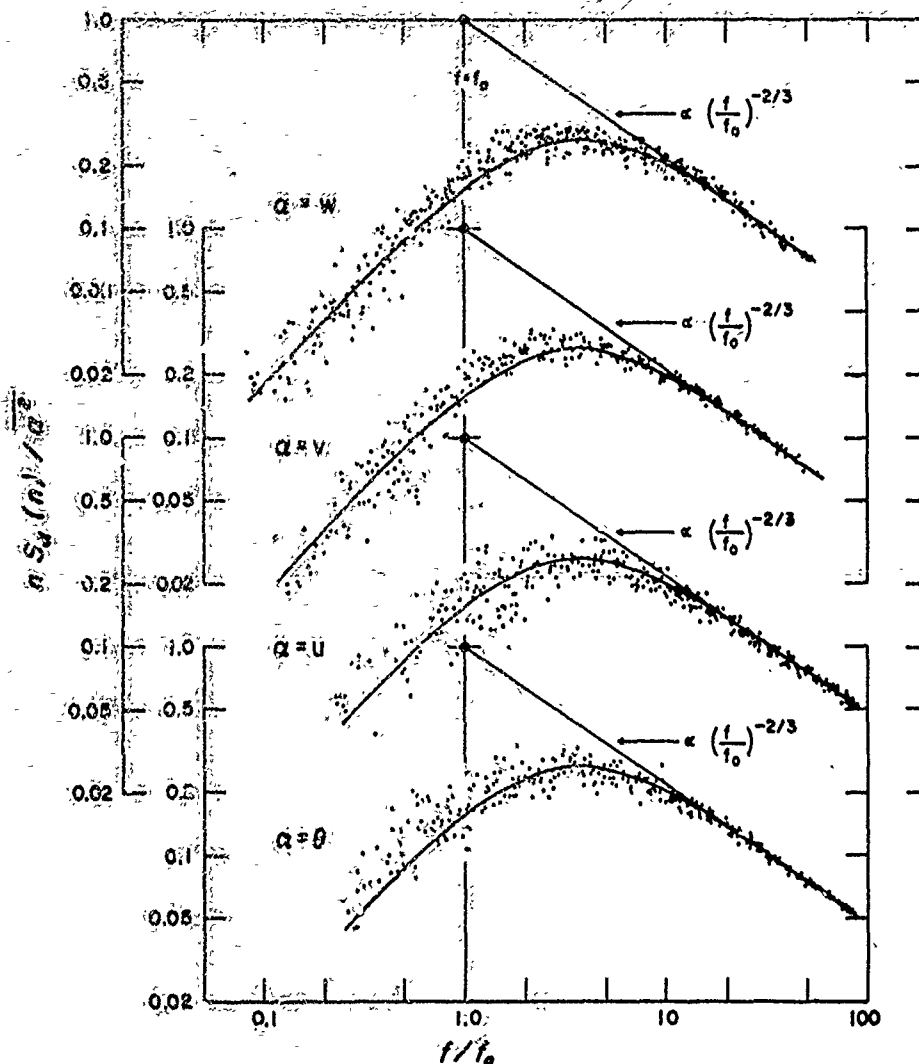


Figure 20. Logarithmic spectra of  $u$ ,  $v$ ,  $w$  and  $\theta$ , normalized by their respective variance, plotted against modified  $f$  scale. Curves shown here correspond to empirical formula in Eq. (23).

approximated empirically by the formula,

$$\frac{nS_{\alpha}(n)}{\alpha^2} = \frac{0.16(f/f_0)}{1 + 0.16(f/f_0)^{2/3}} \quad (23)$$

Once the spectral shape is defined we have a fixed relationship between  $(f_0)_{\alpha}$  and  $(f_m)_{\alpha}$ . From Fig. 20

$$(f_0)_{\alpha} \approx \frac{1}{2}(f_m)_{\alpha} \quad (24)$$

so that Eq. (23) may also be expressed in terms of peak frequency.

We can rearrange the inertial subrange expressions given in Section 4 to obtain another relationship for  $f_0$ . Taking  $w$  as an example we have

$$\frac{nS_w(n)}{\sigma_w^2} = \frac{4\alpha_1/3}{(\sigma_w)^{2/3}} \left(\frac{\epsilon z}{\sigma_w^3}\right)^{2/3} f^{-2/3} \quad (25)$$

where  $\sigma_w$  is the standard deviation of  $w$ . Since  $(f_0)_w$  is, by definition, the  $f$  value when the right-hand side of Eq. (25) is unity

$$(f_0)_w = \frac{1}{2\pi} \left( \frac{4\alpha_1}{3} \right)^{3/2} \left( \frac{\epsilon z}{\sigma_w^3} \right) \approx 0.09 (z/l_w), \quad (26)$$

where  $l_w = \sigma_w^3/\epsilon$ . Using Eq. (24) we have for  $w$

$$(f_m)_{w_c} = z/(\lambda_m)_w = 0.36 z/l_w, \quad (27)$$

so that

$$(\lambda_m)_w \approx 3 l_w. \quad (28)$$

The wavelength corresponding to the peak of the logarithmic  $w$  spectrum in stable conditions is, therefore, three times  $l_w$ . On the basis of experimental results from other turbulent flows (Batchelor 1953), we can indeed expect  $l_w$  to be a length scale characteristic of the energy containing eddies of the  $w$  field.

Expressions similar to Eq. (26) can also be written for  $u$  and  $v$  spectra:

$$(f_0)_v = (f_0)_w \approx 0.09 z/l_v, \quad (29a)$$

$$(f_0)_u = \left( \frac{2}{3} \right)^{3/2} (f_0)_w \approx 0.06 z/l_u, \quad (29b)$$

where

$$l_v = \sigma_v^3/\epsilon \quad \text{and} \quad l_u = \sigma_u^3/\epsilon. \quad (30)$$

For temperature we write from Eq. (9)

$$\frac{nS_\theta(n)}{\sigma_\theta^2} = \frac{\beta_1}{(2\pi)^{2/3}} \left( \frac{N z^{2/3}}{\epsilon^{1/3} \sigma_\theta^2} \right) f^{-2/3}. \quad (31)$$

Again extrapolating this behaviour to the  $nS_\theta(n)/\sigma_\theta^2 = 1$  line gives

$$(f_0)_\theta = \frac{\beta_1^{3/2}}{(2\pi)} \left( \frac{N^{3/2} z}{\epsilon^{1/2} \sigma_\theta^3} \right) \approx 0.11 z/l_\theta, \quad (32)$$

where  $l_\theta = \epsilon^{1/2} \sigma_\theta^3 / N^{3/2}$  is a length scale for temperature analogous to the length scales defined for velocity.

The stable logarithmic cospectra for  $uw$  and  $w\theta$  also exhibit similar shapes when plotted in the same manner as the spectra. In Fig. 21,  $f_0$  is defined by the intercept of the  $-4/3$  inertial subrange slope with the  $nC_{\alpha\beta}(n)/\overline{\alpha\beta} = 1$  line ( $\alpha$  and  $\beta$  are the variables in question and  $\overline{\alpha\beta}$  is the covariance in the frequency bandwidth 0.005 to 10 Hz). A curve that fits both cospectra is

$$\frac{nC_{\alpha\beta}(n)}{\overline{\alpha\beta}} = \frac{0.88(f/f_0)}{1 + 1.5(f/f_0)^{2.1}}, \quad (33)$$

where  $\alpha\beta = uw$  or  $w\theta$ .

The cospectrum of  $u\theta$ , with  $f_0$  redefined by the intercept of the  $-3/2$  inertial subrange slope with  $nC_{u\theta}(n)/\overline{u\theta} = 1$ , may also be represented by a single curve (see Fig. 21)

$$\frac{nC_{u\theta}(n)}{\overline{u\theta}} = \frac{0.85(f/f_0)}{1 + 1.7(f/f_0)^{2.2}}. \quad (34)$$

Using cospectral relationships expressed in Eqs. (13) and (15) and (18) we can write

$$(f_0)_{uw} = 0.10[G(z/L)]^{3/4}, \quad (35a)$$

$$(f_0)_{w\theta} = 0.23[H(z/L)]^{3/4}, \quad (35b)$$

$$(f_0)_{u\theta} = 0.11[K(z/L)]^{2/3} \left[ -\frac{\overline{w\theta}}{\overline{u\theta}} \right]^{2/3}. \quad (35c)$$

The expressions for  $f_0$  in Eqs. (26), (29), (32) and (35) when used in the appropriate interpolation formula give predictions of spectral and cospectral behaviour in the stable

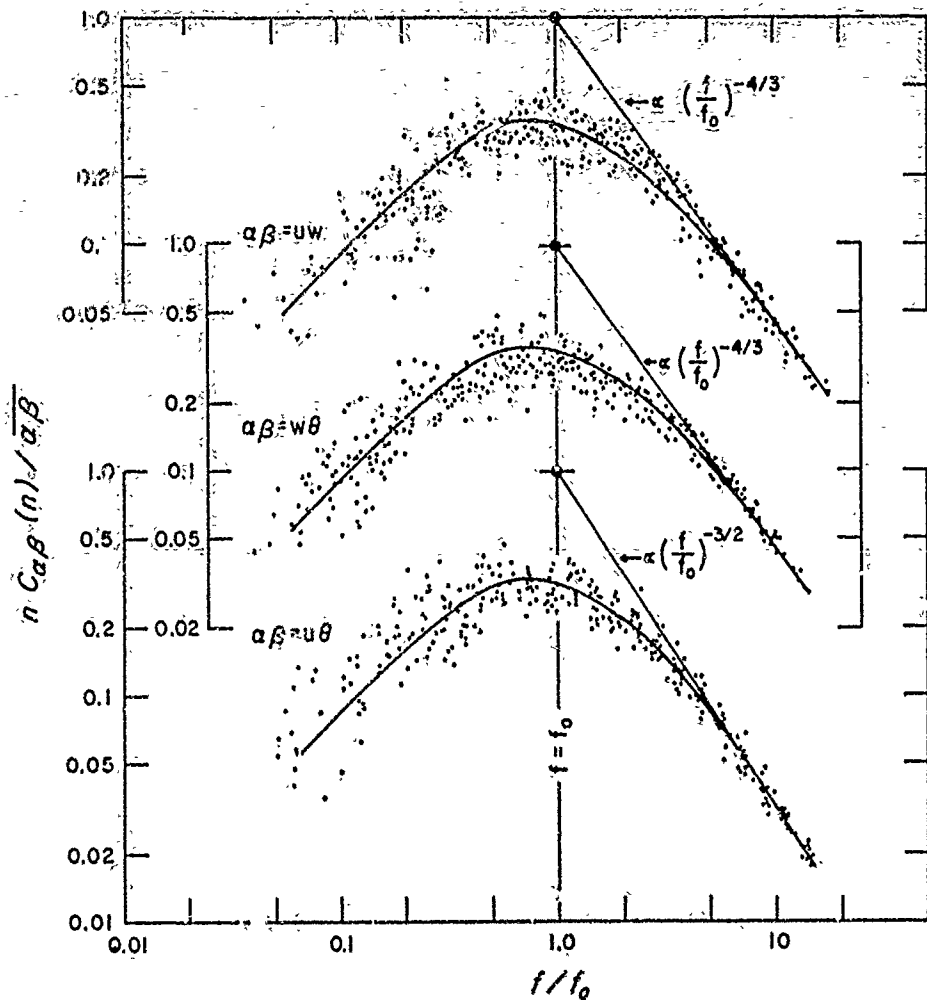


Figure 21. Logarithmic spectra of  $uw$ ,  $w\theta$  and  $u\theta$ , normalized by their covariance, plotted against modified  $f$  scale:  $uw$  and  $u\theta$  curves correspond to Eq. (33);  $w\theta$  curve corresponds to Eq. (34).

surface layer. The unstable spectra might also be formulated in the same manner, but the shapes differ for each parameter, and more complex empirical formulas would be needed (except in  $w$ ) to represent them.

A simple physical model explaining the variation of  $f_0$  with  $z/L$  is given in the companion paper. This model (called local  $z$ -less stratification) predicts that in the very stable limit,  $z$  becomes unimportant and  $L$  is the only significant length scale.  $\lambda_0$ , the wavelength corresponding to  $f_0$ , would therefore be asymptotically proportional to  $L$  and

$$f_0 = z/\lambda_0 \simeq z/L.$$

Fig. 5 in the companion paper shows how  $(f_0)_{uw}$  and  $(f_0)_{w\theta}$  follow the linear prediction, with Eqs. (35a) and (35b) providing the transition to the predicted neutral and unstable behaviour. Such linear trends can be found in the asymptotic behaviour of other  $f_0$ 's as well.

Finally, we should mention that the 'frozen field' expression,  $\kappa_1 = 2\pi n/U$  (or  $f = \kappa_1 z/2\pi$ ) which we have used to convert from frequency to wavenumber is only approximate, particularly at low frequencies. If the conversion were exact, a given turbulence field, whether measured from a fixed tower or a rapidly moving aircraft, would yield the same spectra when plotted against  $f$ . However, Lumley (1965) discusses three

reasons why  $\kappa_1 = 2\pi n/U$  breaks down in high-intensity shear flows: (i) the mean shear causes aliasing; (ii) eddies are continuously changing and are not 'frozen' as they are swept past the instrument; and (iii) smaller eddies are imbedded in larger ones, giving in effect a fluctuating convection velocity. He shows that at high frequencies (inertial range and beyond) only (iii) remains, but this can also be troublesome (Wyngaard and Pao 1972). At low frequencies, all three become significant and it is important to note that the effect of the latter two depends on turbulence level ( $\sigma_u/U$ ). The turbulence level of a given field appears lower to an aircraft observer than to one who is fixed (the aircraft velocity being larger than  $U$ ); so we expect aircraft spectra to be more nearly interpretable as  $\kappa_1$  spectra. Spectral shapes in the low  $f$  range would, therefore, be different for the two observers. Thus, in the energy-containing region,  $U/n$  provides only a rough approximation to the true wavelength.

#### 9. ONSET OF LOCAL ISOTROPY

Although one expects to find isotropy at large  $f$  values, confirmation of this in the first 20 m has been lacking (Kaimal, Borkowski, Panchev, Gjesing and Hasse 1969). For example, the 4/3 ratio between the inertial subrange spectral levels of the transverse and longitudinal velocity components was not found in earlier experiments (Weiler and Burling 1967; Miyake *et al.* 1970). Busch and Panofsky (1968) noted a trend towards the 4/3 ratio in the Round Hill data; more recently Eidsvik and Panofsky (1970) have reported measurements over inhomogeneous terrain which indicate a 4/3 ratio for  $w$  and  $u$  at  $f > 1.0$ . The Kansas data show good agreement with the 4/3 prediction for all but the most stable cases ( $z/L > 1.0$ ). At  $f = 4$ , we find the average spectral ratio to be 1.33 for  $S_w(n)/S_u(n)$  and 1.28 for  $S_v(n)/S_u(n)$ .

The behaviour of  $S_w(n)/S_u(n)$  as a function of  $f$  is particularly revealing (see Fig. 22) since it identifies the onset of the isotropic ratio. (This ratio is established at least an octave sooner in  $S_v(n)/S_u(n)$ , but its onset is not as sharply defined under unstable conditions.) To avoid excessive crowding of data points on the plot, only averaged spectral ratios for the different  $z/L$  categories (see Table 1) are shown.  $S_w(n)/S_u(n)$  increases rapidly in the decade prior to attaining its isotropic value, moving systematically to higher values of  $f$  with increasing  $z/L$ . Only the most stable run clearly falls short of the 4/3 ratio. A unique relationship between the  $u$  and  $w$  spectral cross-over frequency,  $f_c$ , and  $z/L$  is apparent in the data. The plot in Fig. 23 shows  $f_c$  decreasing monotonically in the range  $+2.0 > z/L > -2.0$ , and leveling off to a constant value of nearly 0.2 at  $z/L < 2.0$ . The data points are bounded by  $(f_m)_w$ , the peak frequency of the logarithmic  $w$  spectrum, on the low frequency side and by  $(f_l)_w$ , the lower limit of the  $-5/3$  range in  $w$ , on the high-frequency side.

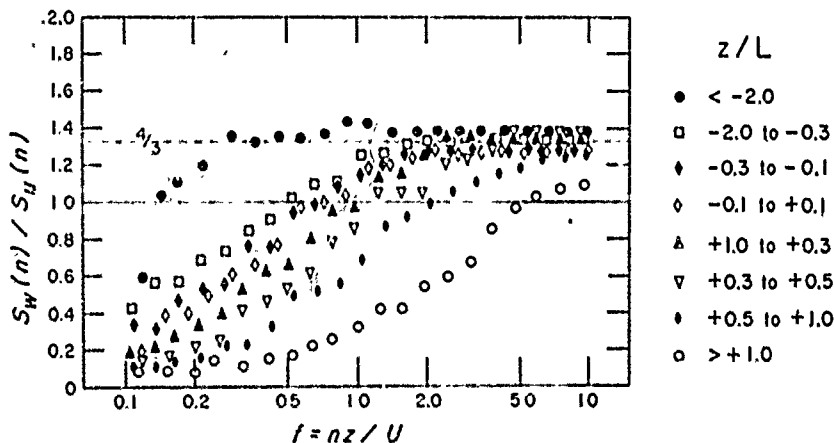


Figure 22. Plot of the ratios of  $w$  and  $u$  spectral estimates showing approach to the 4/3 ratio required for isotropy.



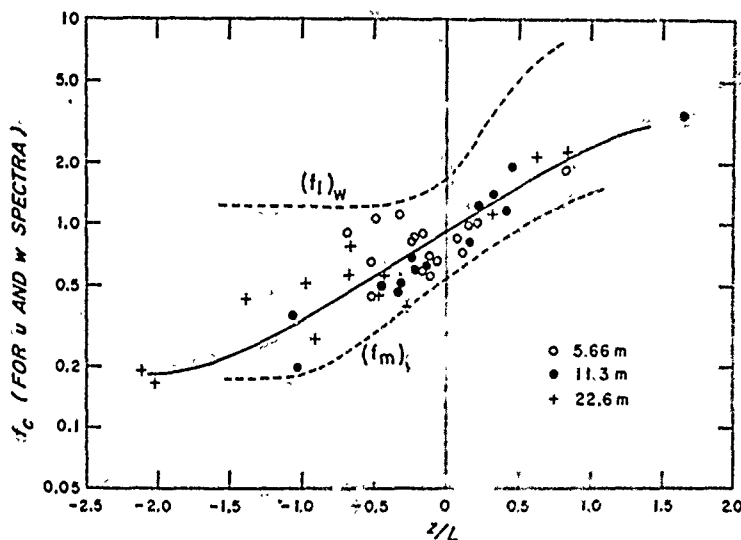


Figure 23. Crossover frequency,  $f_c$ , for  $u$  and  $w$  spectra plotted against  $z/L$ . Solid curve is fitted by eye; dashed curves indicate upper and lower bounds for  $f_c$ .

At  $f > (f_l)_w$ , therefore, all three velocity components have  $-5/3$  spectral slopes and the spectral ratios predicted by isotropy. Furthermore, at  $(f_l)_w$  both the  $w\theta$  and  $uw$  cospectra are falling rapidly (as the  $-7/3$  power) to zero. We can, therefore, drop the subscript  $w$ , and treat  $f_l$  as the lower limit of the locally isotropic range. From Fig. 23,  $f_l$  is a constant ( $\approx 1.2$ ) for  $z/L < 0$ , and approaches  $10 z/L$  for  $z/L > 0$ . The limiting streamwise wavelength is, therefore, of the order of  $z$  under unstable conditions and  $L/10$  under stable conditions.

The observed variation of  $f_l$  with  $z/L$  is consistent, as we will now show, with arguments put forth by Lumley and Panofsky (1964). Since anisotropy results from wind shear and buoyancy, they suggest that only eddies with time scales small compared to the time scales of shear and buoyancy will be isotropic. A suitable eddy time scale is

$$\tau = (\kappa^3 E)^{-1/2} \quad (36)$$

where  $E$  is the three-dimensional spectrum; it represents the density of contributions to turbulent kinetic energy from wave numbers of magnitude  $\kappa$ . We expect the onset of isotropy to occur in the  $\kappa^{-5/3}$  range of  $E$ , so Eq. (36) may be expressed as

$$\tau = \alpha^{-1/2} \epsilon^{-1/3} \kappa^{-2/3} \quad (37)$$

where  $\alpha$  is the three-dimensional spectral constant. As expected, this time scale decreases with eddy size.

There are two buoyancy time scales, one associated with the mean temperature change with height and one caused by temperature fluctuations. Including shear we now have three significant external time scales:

$$\tau = \left(\frac{dU}{dz}\right)^{-1} \quad (\text{mean shear}) \quad (38a)$$

$$\tau = \left(\frac{\theta}{g}\right)^{1/2} \left|\frac{d\theta}{dz}\right|^{-1/2} \quad (\text{mean buoyancy}) \quad (38b)$$

$$\tau = \left(\frac{\theta}{g}\right) \left(\frac{\epsilon}{N}\right)^{1/2} \quad (\text{fluctuating buoyancy}) \quad (38c)$$

We expect isotropy for wave numbers where the eddy time scale in Eq. (37) is small

compared to the time scales in Eq. (38). The criteria for isotropy become

$$\kappa > \alpha^{-3/4} \epsilon^{-1/2} \left( \frac{dU}{dz} \right)^{3/2} \quad (39a)$$

$$\kappa > \alpha^{-3/4} \epsilon^{-1/2} \left( \frac{z}{\theta} \right)^{3/4} \left| \frac{d\theta}{dz} \right|^{3/4} \quad (39b)$$

$$\kappa > \left( \frac{g}{\theta} \right)^{3/2} \left( \frac{N}{\epsilon^{2/3}} \right)^{3/4} \quad (39c)$$

Although these criteria are derived for three-dimensional spectra, they should be applicable to one-dimensional spectra as well. In order surface-layer terms, they can be expressed as

$$f > 0.3 \phi_m^{3/2} \phi_\epsilon^{-1/2} \quad (\text{mean shear}) \quad (40a)$$

$$f > 0.3 \left| \frac{z}{L} \right|^{3/4} \phi_N^{3/4} \phi_\epsilon^{-1/2} \quad (\text{mean buoyancy}) \quad (40b)$$

$$f > 0.3 \left| \frac{z}{L} \right|^{3/2} \phi_N^{3/4} \phi_\epsilon^{-5/4} \quad (\text{fluctuating buoyancy}) \quad (40c)$$

Under very unstable conditions the buoyancy criteria dominate, and in the  $\lambda \ll z$ -convective limit they give  $f > 0.1$ . In neutral conditions only the shear criterion is operative, and it gives  $f > 0.3$ . Under stable conditions all three become proportional to  $z/L$ ; here shear is the most restrictive, giving  $f > 1.4 z/L$ . Therefore, we expect  $f_t$  to approach a constant under very unstable conditions, and to vary as  $z/L$  on the stable side. Our observations, Fig. 23, clearly support this prediction, and suggest that we can interpret  $>$  in our inequalities as meaning greater by a factor of 5 – 10.

## 10. CONCLUSIONS

The spectra and cospectra of velocity and temperature fluctuations show systematic behaviour with  $z/L$  when expressed in appropriate similarity co-ordinates. All spectra and cospectra reduce to a family of curves which converge into single universal curves in the inertial subrange but spread out according to  $z/L$  at lower frequencies. Other data obtained in recent years over land and water fit the composite curves reasonably well.

The high-frequency behaviour is consistent with local isotropy. In the inertial subrange, where the spectra fall as  $n^{-5/3}$ , the cospectra fall faster:  $uw$  and  $w\theta$  as  $n^{-7/3}$ , and  $u\theta$ , on the average as  $n^{-5/2}$ . The 4/3 ratio between the transverse and longitudinal velocity spectral levels is observed at wavelengths of the order of  $z$  under unstable conditions and about  $L/10$  under stable conditions.

The spectral constant  $\alpha_1$  agrees well with other experimental data, but additional research is needed to resolve the discrepancy between our (indirect)  $\beta_1$  value and recent directly-measured values.

## ACKNOWLEDGMENTS

We gratefully acknowledge the contributions of all members of the Boundary Layer Branch at ARFCL to the experimental and data analysis efforts which made this paper possible. Also, our thanks to Mr. Richard D. Sizer for redrawing the Figures and to Miss Suzanne C. Tourville for typing the manuscript.

## REFERENCES

- Batchelor, G. K. 1953 'The theory of homogeneous turbulence, Cambridge University Press, Cambridge, England, 197 pp.

- Berman, S. 1965 'Estimating the longitudinal wind spectrum near the ground,' *Quart. J. R. Met. Soc.*, **91**, pp. 302-317.
- Bradley, E. F. 1968 'A shearing stress meter for micro-meteorological studies,' *Ibid.*, **94**, pp. 380-387.
- Boston, N. 1970 'An investigation of high wave number temperature and velocity spectra in air,' *Ph.D. Thesis, University of British Columbia*.
- Rusch, N. E. and Panofsky, H. A. 1968 'Recent spectra of atmospheric turbulence,' *Quart. J. R. Met. Soc.*, **94**, pp. 132-148.
- Businger, J. A., Wyngaard, J. C., Izumi, Y. and Bradley, E. F. 1971 'Flux-profile relationship in the atmospheric surface layer,' *J. Atmos. Sci.*, **28**, pp. 181-189.
- Corrsin, S. 1951 'On the spectrum of isotropic temperature fluctuations in an isotropic turbulent flow,' *J. Appl. Phys.*, **22**, pp. 469-473.
- Cramer, H. E. and Record, F. A. 1969 'Properties of turbulent energy spectra and cospectra in the atmospheric surface layer,' *Final Report ECOM-64-G1-F M.I.T., Dept. of Met.*
- Eidsvik, K. J. and Panofsky, H. A. 1970 'Turbulence measurements over inhomogeneous terrain,' *Internal Report, Norwegian Defence Research Establishment, Norway*, 41 pp.
- Elderkin, E. C. 1966 'Experimental investigation of the turbulence structure in the lower atmosphere,' *AEC Research and Development Report, BNWL-329, Battelle Northwest Laboratory, Hanford, Washington*.
- Gibson, C. H. and Schwarz, W. H. 1963 'The universal equilibrium spectra of turbulent velocity and scalar fields,' *J. Fluid Mech.*, **16**, pp. 365-384.
- Gibson, C. H., Stegen, G. R. and Williams, R. B. 1970 'Statistics of the fine structure of turbulent velocity and temperature fields measured at high Reynolds number,' *Ibid.*, **41**, pp. 153-167.
- Grant, H. L., Hughes, B. A., Vogel, W. M. and Moilliet, A. 1968 'The spectrum of temperature fluctuations in turbulent flow,' *Ibid.*, **34**, pp. 423-442.
- Haugen, D. A., Kaimal, J. C. and Bradley, E. F. 1971 'An experimental study of Reynolds stress and heat flux in the atmospheric surface layer,' *Quart. J. R. Met. Soc.*, **97**, pp. 168-180.
- Izumi, Y. 1971 'Kansas 1968 field program data report,' *Environmental Research Papers, No. 379, AFCRL-72-0041, Air Force Cambridge Research Laboratories, Bedford, Massachusetts*.
- Kaimal, J. C. 1969 'Measurement of momentum and heat flux variations in the surface boundary layer,' *Radio Sci.*, **4**, pp. 1,147-1,153.
- Kaimal, J. C., Borkowski, J., Panchev, S., Gjessing, D. T. and Hasse, L. 1969 'Anisotropy of the fine structure,' *Ibid.*, **4**, pp. 1,369-1,370.
- Kaimal, J. C. and Businger, J. A. 1970 'Case studies of a convective plume and a dust devil,' *J. Appl. Met.*, **9**, pp. 612-620.
- Kaimal, J. C. and Haugen, D. A. 1967 'Characteristics of vertical velocity fluctuations observed on a 430 m tower,' *Quart. J. R. Met. Soc.*, **93**, pp. 305-317.
- 1969 'Some errors in the measurement of Reynolds stress,' *J. Appl. Met.*, **8**, pp. 460-462.
- Kaimal, J. C., Haugen D. A. and Newman, J. T. 1966 'A computer controlled mobile micro-meteorological observation system,' *Ibid.*, **5**, pp. 411-420.
- Kaimal, J. C., Wyngaard, J. C. and Haugen, D. A. 1968 'Deriving power spectra from a three-component sonic anemometer,' *Ibid.*, **7**, pp. 827-837.
- Kukharets, V. P. and Tsvang, L. R. 1969 'Spectra of turbulent heat flux in the atmospheric boundary layer,' *Izv. Atmos. Oceanic Phys.*, **5**, pp. 1,132-1,142.
- Lumley, J. L. 1965 'Interpretation of time spectra measured in high intensity shear flows,' *Physics Fluids*, **8**, pp. 1,056-1,062.
- Lumley, J. L. and Panofsky, H. A. 1964 *The structure of atmospheric turbulence*, New York, Interscience, 239 pp.
- McBean, G. A. 1970 'The turbulent transfer mechanisms in the atmospheric surface layer,' *Ph.D. Thesis, University of British Columbia, Canada*.
- Miyake, M., Stewart, R. W. and Burling, R. W. 1970 'Spectra and cospectra of turbulence over water,' *Quart. J. R. Met. Soc.*, **96**, pp. 138-143.
- Panofsky, H. A. 1969 'The spectrum of temperature,' *Radio Sci.*, **4**, pp. 1,143-1,146.

- Panofsky, H. A. and Mares, E. 1968 'Recent measurements of cospectra for heat flux and stress,' *Quart. J. R. Met. Soc.*, **94**, pp. 581-584.
- Paquin, J. E. and Pond, S. 1971 'The determination of the Kolmogoroff constants for velocity, temperature and humidity fluctuations from second- and third-order structure functions,' *J. Fluid Mech.*, **50**, pp. 257-269.
- Phelps, G. T. and Pond, S. 1971 'Spectra of the temperature and humidity fluctuations and of the fluxes of moisture and sensible heat in the marine boundary layer,' *J. Atmos. Sci.*, **28**, pp. 918-928.
- Sitaraman, V. 1970 'Spectra and cospectra of turbulence in the atmospheric surface layer,' *Quart. J. R. Met. Soc.*, **96**, pp. 744-749.
- Weiler, H. S. and Burling, R. W. 1967 'Direct measurements of stress and spectra of turbulence in the boundary layer over the sea,' *J. Atmos. Sci.*, **24**, pp. 652-664.
- Wyngaard, J. C. and Coté, O. R. 1971 'The budgets of turbulent kinetic energy and temperature variance in the atmospheric surface layer,' *Ibid.*, **28**, pp. 190-201.
- 1972 'Spectral similarity in the atmospheric surface layer,' *Quart. J. R. Met. Soc.*, **98**, pp. 590-603.
- Wyngaard, J. C., Coté, O. R. and Izumi, Y. 1971 'Local free-convection, similarity and the budgets of shear stress and heat flux,' *J. Atmos. Sci.*, **28**, pp. 1,171-1,182.
- Wyngaard, J. C. and Lumley, J. L. 1967 'A sharp cut-off spectral differentiator,' *J. Appl. Met.*, **6**, pp. 952-955.
- Wyngaard, J. C. and Pao, Y. H. 1972 'Some measurements of the fine structure of large Reynolds number turbulence,' *Proceedings, Symposium on Statistical Models and Turbulence, La Jolla, Cal. 1971.*, Springer-Verlag, Berlin, pp. 384-401.
- Zubkovsky, S. L. and Koprov, B. M. 1969 'Experimental investigation of the structure of the turbulent heat and momentum fluxes in the atmospheric surface layer,' *Izv. Atmos. Oceanic Physics*, **5**, pp. 323-331.